PHYSICAL REVIEW A VOLUME 24, NUMBER 1 JULY 1981

Electrostatic instabilities of a finite electron beam propagating in a cold magnetized plasma

D. Le Queau and R. Pellat*
Centre de Physique Théorique de l'Ecole Polytechnique, 91128 Palaiseau Cedex, France

A. Saint Marc
CESR, Centre National de la Recherche Scientifique Boîte Postale 4346, 31029 Toulouse, Cedex, France
(Received 18 July 1980)

For a better understanding of the high-frequency waves observed during active experiments of electron-beam injection into the ionospheric plasma, we do a complete investigation of the electrostatic-beam–plasma instabilities that do occur in such a situation. The electron beam is cold, it is aligned with the vacuum magnetic field, and has a finite radius; the background plasma is cold and homogeneous. We study both analytically and numerically the dispersion equation of the different branches and follow the dependence of the temporal and spatial growth rates with the beam and plasma parameters. Simultaneously we investigate the different types of instabilities (radiated or confined to the beam) in the various frequency ranges which are of interest. We give an analytical criterion for the convective or absolute character of these instabilities, taking into account the two-dimensional wave propagation along and across the vacuum magnetic field.

INTRODUCTION

Beam-plasma instabilities have already been the subject of many experimental and theoretical works. Their linear and nonlinear behavior is of great importance in plasma physics. The main motivation of their study was found in traveling-wave tubes and also in fusion research. More recently it has been suggested that "coherent" natural radio emissions are mainly produced by beam-plasma instabilities. Space exploration by rockets and satellites give, in some cases, a direct evidence of this relationship, i.e., for the so-called interplanetary type-III bursts (of solar origin) or for planetary emissions (the kilometric earth radiation or the Jovian decametric radiation).

Beside these natural emissions, active experiments are now currently performed in the ionospheric plasma mainly with electron guns of rocket payloads aboard.[1,2] In the near future, similar experiments will be achieved with the space-shuttle facilities. Let us recall the main features of these experiments. The ionospheric background plasma is magnetized, cold, and "infinite". The electron beams are cold and energetic (in the range of 10 keV), and they have finite transverse dimensions, the measurements are made far from the beam, within kilometers as compared with a beam radius of ten meters or less. Some of them are also made from the ground at a few hundred kilometers. These working conditions are somewhat different from standard laboratory conditions. This explains why most of the results of active experiments performed with electron beams were unexpected. From the results of the theoretical work performed with these experimental conditions[3] one did not expect observable emissions related to the beam-plasma instabilities: The only instable modes were found to be confined in the beam vicinity and only produced in the nonpropagative frequency gap $\omega_c < \omega < \omega_p$ (ω_c is the electronic cyclotron frequency and ω_p is the electronic plasma frequency). No measurements were made in the beam vicinity but emissions were observed far from the electron beam, which disagrees with the previously quoted theoretical result.

The results of the wave measurements made in the ionospheric plasma clearly indicate a band of quasielectrostatic waves in the lowest-frequency "window" $0 < \omega < \omega_c$ and also a band of emissions in the window $\omega_p < \omega < \omega_H$ [$\omega_H = (\omega_p^2 + \omega_c^2)^{1/2}$ is the upper hybrid frequency]. These high-frequency emissions have only been recorded with electrostatic antennas and show both transient and continuous temporal evolution.[1,2,4-6,7(a)-7(c)]

Electromagnetic emissions have also been registered on the ground at a frequency which corresponds roughly to $2\omega_c$, the gyrofrequency being taken at the altitude of injection (usually between 150 kM and a few hundred kilometers).[4] From these results it is obvious that our theoretical understanding of a beam-plasma system is insufficient. The observed, very small beam dispersion in velocity space a few eV is a common feature of active experiments in space. This feature gives the possibility of a spatial particle bunching which has already been analyzed elsewhere[5,6] and may explain some of the experimental observations, especially in the frequency range $\omega_p < \omega < \omega_H$. Nevertheless, the origin of most of the observed emissions is certainly to be found in a linear-beam-plasma instability[8] or in its nonlinear consequences. Thus, in the lowest-frequency range $0 < \omega < \omega_c$, two possibilities have already

been proposed: a linear quasielectrostatic instability[9] and a nonlinearly radiated quasielectrostatic wave produced by the beats of two high-frequency quasielectrostatic modes in the ω_p range.[7(d),10]

In such a complex experimental situation it seems necessary to proceed systematically. The first natural step is obviously to get a better understanding of the linear-instability theory and of their nonlinear evolution. The progress achieved among active experiments (laboratory experiments are no longer undertaken in this field) will also allow a better understanding of natural radio-emission processes.

In this first paper we limit our investigation to the case of a monoenergetic, nonrelativistic electron beam with finite transverse dimension, injected parallel to the external magnetic field in a cold infinite homogeneous plasma. Our stability analysis is performed with the classical quasielectrostatic approximation. This approximation is valid for parallel beams (with beam and plasma parameters relevant to active ionospheric experiments) only, since electromagnetic instabilities are expected for oblique injection.

For the sake of clarity let us summarize the principal feature of our model, together with the terminology we shall use in this paper. The dispersion relation of quasielectrostatic plane waves in a magnetized cold uniform plasma reads simply

$$k_{\parallel}^2(1-\omega_p^2/\omega^2)+k_{\perp}^2\,[1-\omega_p^2/(\omega^2-\omega_c^2)]=0\,,$$

where $k_{\parallel}$ and $k_{\perp}$ are, respectively, the parallel and perpendicular wave numbers with respect to the external field. We deduce from the above formula two propagating windows (Fig. 1), $0<\omega<\omega_c$ and $\omega_p<\omega<\omega_H$, which are complementary to two nonpropagative frequency ranges $\omega_c<\omega<\omega_p$ and $\omega>\omega_H$.

The spectrum of the transverse wave number is continuous for an infinite plasma, while it is discrete when the plasma is confined in a wave guide. Here the transverse wave number is quantized through adapted boundary conditions. This quantization, which has been used in many thorough investigations,[11-14] is clearly not adapted to the physical situation we are dealing with. Nevertheless, we shall encounter a sort of quantization of the internal (with respect to the beam's volume) wave number, due to the reflecting properties of the beam's radial boundaries. This determines the stability of the transverse spatial structure of the wave-equation solution as frequency or other parameters are changed.

Let us now add to this infinite plasma an electron beam on a cylindrical subset of field lines. The beam generates waves which remain confined to its vicinity in the nonpropagative frequency gap $\omega_c<\omega<\omega_p$ and $\omega>\omega_H$. They have been previously studied in Ref. 3. However, the beam should also pick up propagating solutions in the continuous-plasma wave spectrum. For radially confined beam modes one expects $|\mathrm{Im}k_r|\gg\mathrm{Re}\,k_r$ (k_r is a "radial" wave number). On the contrary, one expects $\mathrm{Re}\,k_r\gg|\mathrm{Im}k_r|$ for a propagating mode. In addition to that classification which involves the external structure of the solution, we shall show a further distinction between Cherenkov and slow (or fast) cyclotronic branches, depending on the resonance line $\omega=k_{\parallel}V_b$ or $\omega=k_{\parallel}V_b\pm\omega_c$ (where V_b is the beam's velocity, and $k_{\parallel}$ the axial wave number) which plays the principal role in determining the instability of the studied branches. Moreover, as already pointed out, we must also pay attention to the internal structure of the solution (behavior of the potential inside the beam). We shall classify the solutions with respect to the number of internal nodes of the potential. For zero-node solutions another distinction has to be made between body and surface branches (Fig. 2).

This paper is organized in the following way:

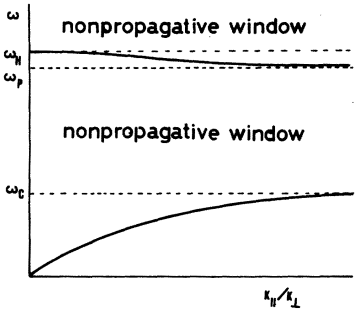

FIG. 1. Dispersion relation of quasielectrostatic plane wave in a magnetized cold uniform plasma.

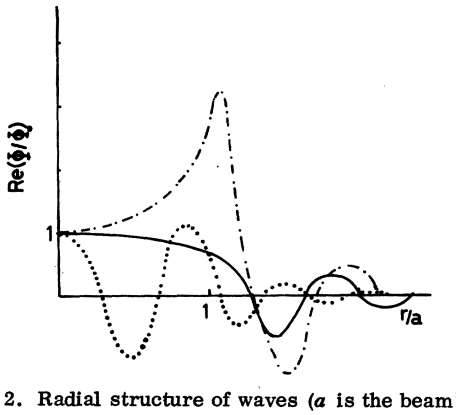

FIG. 2. Radial structure of waves (a is the beam's radius): —— zero-node body mode, – – – zero-node surface mode, and ··· two-node mode.

In Sec. I we shall justify the use of our model in the physical situation of active-injection experiments, and introduce the mathematical tools. In Sec. II, we solve our set of equations in the low-frequency propagative range ($\omega < \omega_c$). In Sec. III, we study some systems of equations in the higher-frequency ranges. One finds a detailed study of the convective or absolute character of the instabilities there. The appendices are devoted to the details of the algebra. Our study includes, in all, frequency windows, the Cherenkov branches, and the slow (or fast) cyclotronic branches. We also demonstrate the absence of instabilities for $\omega > \omega_H$.

I. THE MODEL: A COLD MAGNETIZED BEAM STREAMING IN AN INFINITE HOMOGENEOUS PLASMA

A. Physical consistency

Our model is somewhat simple compared to the real geometry of the electron beam injected into the ionospheric plasma, and to the real conditions that will be encountered in such a medium. Let us summarize its principal features. We take a cylindrical cold electron beam of radius a, which flows with a constant velocity V_b along a constant magnetic field (electronic cyclotron frequency ω_c) in which all the infinite surrounding plasma is immersed. The ratio between the beam density n_b and the plasma density n_p (which are related to plasma frequencies ω_b and ω_p) is a small parameter ϵ. The ionospheric ions are taken as a neutralizing motionless background, which limits our results to frequencies higher than the lower hybrid frequencies. The plasma is taken to be cold and noncollisional. Noncollisional dissipation processes such as Landau damping are also neglected. For the stability analysis we take the quasistatic approximation.

To justify these assumptions let us now specify the choice of the beam and plasma parameters, bearing in mind the use of our model in the framework related to wave observations carried out during an ionospheric active experiment such as the ARAKS one.[7] When the beam is injected at some angle with respect to the earth's magnetic field, we do not know its real structure. As a result of the neutralizing process, it can keep helical structure or become cylindrical.[5] The relevant generalization of the Brillouin's model has not yet been computed and the beam structure has not been measured in the experiments already performed. Our knowledge will be improved in future experiments expected on the space shuttle. For our computations, we take a cylindrical beam flowing along a uniform magnetic field through a homogeneous plasma. This model is justified by the results of the wave experiments which seem to be qualitatively independent of the angle of injection. To simulate the different angles of injection and the consecutive extension of the beam's radius we take different beam radii a between the Brillouin radius $r_B = [2e/\pi(2m_e)^{1/2}\epsilon_0\omega_c^2]^{1/2} I^{1/2} E^{-1/4}$ and the cyclotronic radius $r_{ce} = (2/m_e\omega_e^2)^{1/2} E^{+1/2}$, where E is the beam energy, I is the injection current, and e and m_e are the charge and mass of the electron. For our ionospheric parameters one obtains $2.5E^{-1/4}I^{1/2} \leq a \leq 10E^{1/2}$ (the beam energy E has been scaled to 10^4 eV, I is in A, and a is in meters). In that modeling, the ratio ϵ between beam and plasma densities is simply scaled through the important plasma parameter ω_c/ω_p, which will be noted α_c in the following: For the Brillouin flow we obtain $\epsilon = \alpha_c^2/2$, while for a beam with cyclotronic radius $\epsilon = 3 \times 10^{-2} \alpha_c^2 I/E^{3/2}$ (with the same scaling as above for beam energy E and current I), with relevant injection parameters (E = 30–15 keV and I = 0.5 A), we obtain the beam's radius varying from 1 to 10 m and ϵ/α_c^2 from 0.5 (Brillouin flow) to 5×10^{-3}.

In a typical active experiment the ionospheric plasma frequency changes more rapidly during the rocket flight than the electronic cyclotron frequency.[7] We take $\omega_p \sim 2\pi \times 4$ MHz [which corresponds to the apogee of the so-called North flight of the ARAKS experiment (~300 km)] to $\omega_p \sim 2\pi \times 2.5$ MHz (end of the active part of the flight). These values correspond, respectively, to $n_p \sim 2 \times 10^5$ and 7×10^4 cm^{-3}. The gyrofrequency lies very close to $\omega_c \sim 2\pi \times 1.2$ MHz. This situation corresponds to α_c varying between $\alpha_c \sim 0.3$ (apogee) to $\alpha_c \sim 0.5$ (end of the flight). With these values of the relevant parameters the classical growth rate of the beam-plasma instability, $\gamma/\omega_p \sim (\omega_b/\omega_p)^{2/3} \sim 0.2 I^{1/3} E^{-1/2}$, is rather insensitive to the injection parameters. This is in agreement with the great similarity between the results of various wave measurements performed during different experiments, despite the broad range of the injection currents.

The temperature of the ionospheric plasma is very small (typically of the order of 0.1 eV) and negligible, even as far as the properties of the group velocity of the excited waves are concerned. This is a consequence of a magnetized beam. This point leads us to neglect, in our stability analysis, the usual dissipative processes [collisional and noncollisional (Landau) damping], even for the upper hybrid branch ($\omega_p < \omega < \omega_H$) where the smallness of the group velocity leads generally to strong spatial damping. As we shall show, both numerically [see Figs. 3(a), 4(b), 5, and 6(b)] and analytically [Eq. (C4) of Appendix C], the electro-

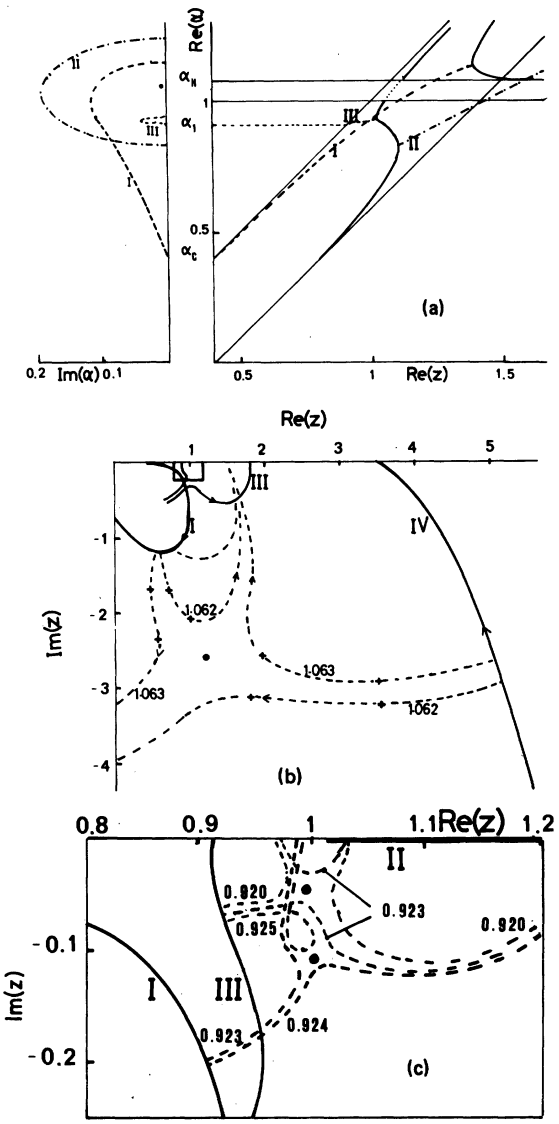

FIG. 3. The zero-one node sheet for $\epsilon=\alpha_c^2/2$ ($\alpha_c=0.4$). (a) Re(z) or complex (α), (b) complex-z mapping [continued lines are solution with Im $\alpha=0$, dotted lines are solutions with Re $\alpha=cte$ (indicated by the number), and crosses are separated by $\Delta(\mathrm{Im}\,\alpha)=5\times10^{-3}$], and (c) vicinity of $\alpha_1=0.909$.

static waves generated in our model may become absolutely instable at a frequency very close to the upper hybrid frequency ω_H. To play a significant role in our stability analysis, any temporal damping rate (say γ_d) must be of the order of the imaginary part of the frequency at this particular point.

As we are dealing with Cherenkov or cyclotronic branches (with $\omega_c \ll \omega_p$), which involves $\omega \sim k_\parallel V_b$, the temporal damping rates associated with noncollisional dissipation processes are scaled by quantities of the form $\exp(-z_i^2)$ where $z_i \sim [(\omega - l\omega_c)/$

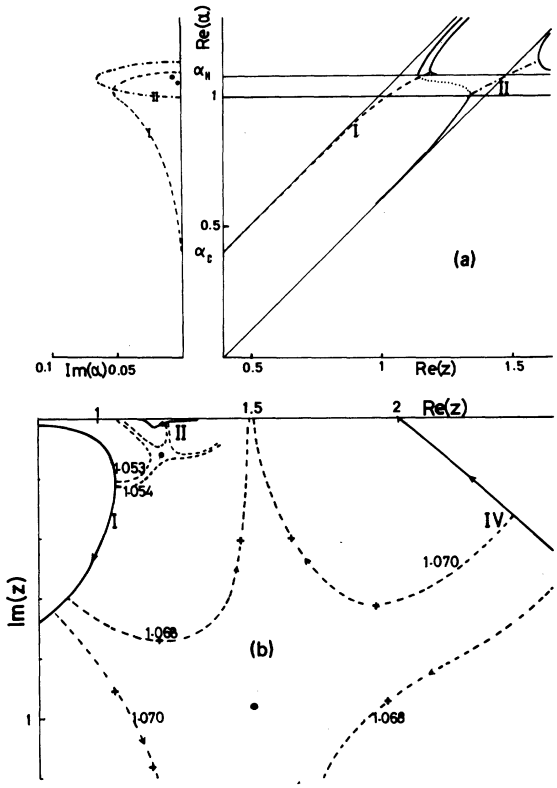

FIG. 4. (a) and (b) The one-two node sheet for $\epsilon=\alpha_c^2/20$ ($\alpha_c=0.4$).

$\omega] V_b/V_{th}$ (where V_{th} is the thermal velocity of the plasma). In our case these quantities have dimensions of $\sim\exp\{-10^{+5}[(\omega - l\omega_c)/\omega]^2\}$ with $\omega \sim \omega_p$. This is always very small.

At the altitude where the wave measurements are made the electron-ion collisions are predominant. We expect a collisional damping rate of the order of the electron-ion collision frequency which

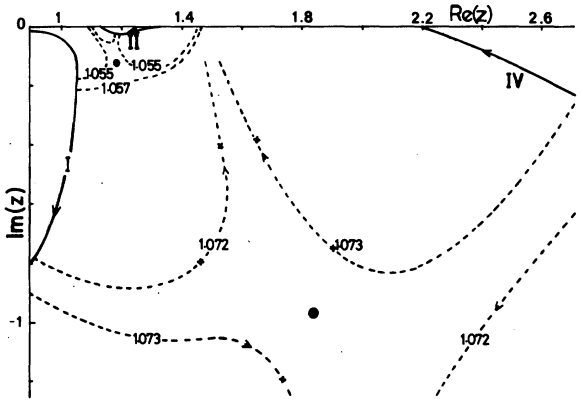

FIG. 5. The two-three node sheet for $\epsilon=\alpha^2/20$ ($\alpha_c=0.4$).

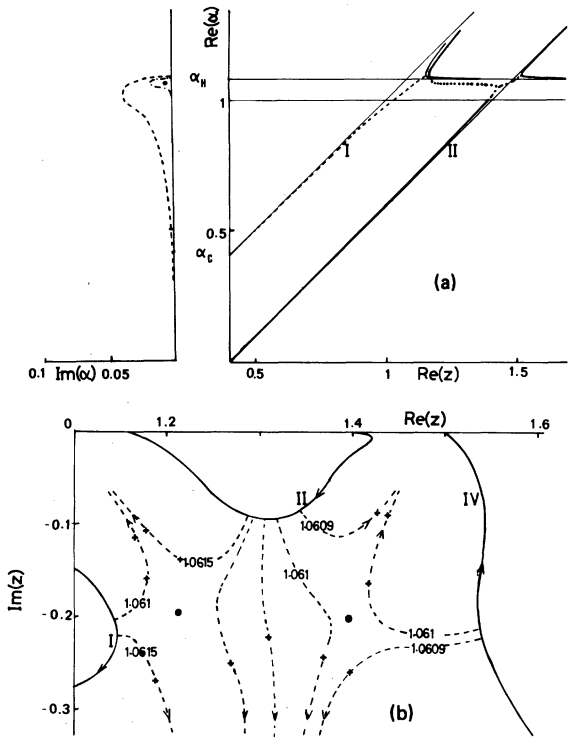

FIG. 6. (a) and (b) Two-three node sheet for $\epsilon = \alpha_c^2/200$ ($\alpha_c = 0.4$).

is about 200 Hz. Conveniently scaled with the plasma frequency $\gamma_{\text{coll}}/\omega_p \sim 5\times10^{-5}$. This has to be compared with the computed values of $\text{Im}\omega/\text{Re}\omega \gtrsim 5\times10^{-3}$ for the cases numerically investigated in that paper. These comparisons justify neglecting the usual dissipative processes in our stability analysis.

Nevertheless, we see from formula (C4b) of Appendix C that, for small radial wavelengths in the beam's interior, the excited waves may be stabilized when

$$2\pi\lambda_\perp^{\text{in}}\left(\frac{n_b}{n_p}\right)^{1/2} \lesssim \frac{\gamma_{\text{coll}}}{\omega_p}\frac{V_b}{\omega_p}\frac{\omega_c}{\omega_p}\,.$$

With our particular choice of parameters, this arises for $\lambda_\perp^{\text{in}}(n_b/n_p)^{1/2} \lesssim 4\times10^{-4}$ m. This implies a very small wavelength (with respect to beam radius), and the most amplified modes (which arises for internal perpendicular wavelengths which are only a small fraction of the beam radius) shall not be perturbed by dissipation processes. Moreover, the energy spread of the electron beam is known to be negligible in the computation of the instabilities growth rate as long as $\gamma/\omega_p > (\Delta E/E)^{1/2}$, a condition which is satisfied with a typical value $(\Delta E/E)^{1/2} \sim 10^{-2}$ for $I > 10^{-3}$ A, which covers all experiments.

Since we have justified the use of our model to investigate the properties of the electrostatic waves which can be excited by the beam a few words have to be said about possible electromagnetic emissions. With an off-angle beam propagation, electromagnetic instabilities are well known.[15] These instabilities may explain the emissions observed from the ground[2,4] during the operation of the electron gun from the rocket payload. A relevant treatment under these experimental conditions is left for further work. From the measurements of the wave spectrum performed *in situ* in the ARAKS experiment[2,16] the electrostatic approximations have been verified. Let us recall that the difference between quasistatic and electromagnetic waves is mainly provided by the difference between index of propagation: Electromagnetic waves have an index of propagation of the order of unity. The quasielectrostatic approximation (exact in the vicinity of the resonance cones) holds for an index of propagation much larger than unity.

From previous works we know that the quasistatic approximation gives correct results when the energy of the beam's electrons is low,[17] typically below 80 keV (and of course when low-phase-velocity waves are studied). Furthermore, when the beam's radius and cyclotron electronic frequency are relatively low [typically when $(a\omega_c/c) < 1$] quasistatic results give the correct negative slope for the upper-frequency-plasma branch[17] $[\omega_p < \omega < \omega_H = (\omega_p^2 + \omega_e^2)]$, thus giving rise to the possibility of nonconvective instability by a backward-oscillation mechanism.

B. Mathematical tools

We start from the usual system of beam- and cold-plasma electron fluid equation, together with the Poisson equations

$$\frac{\partial n_j}{\partial t} + \vec{\nabla}\cdot(n_j\vec{V}_j) = 0\,,$$

$$\frac{\partial \vec{V}_j}{\partial t} + \vec{V}_j\cdot\nabla\vec{V}_j = -\frac{e}{m_e}(\vec{E} + \vec{V}_j\times\vec{B})\,,$$

$$\vec{\nabla}\cdot\vec{E} = -\Delta\Phi = -\sum n_j\frac{e}{\epsilon_0}\,.$$

$j = b, p$ for the beam and plasma electrons, respectively.

After a standard linearization of these equations, one obtains the system of partial differential equations which describe the wave properties. In a cylindrical system of coordinates (r, θ, z), convenient for the geometry of the system, we limit our work to axisymmetric solutions $(\partial/\partial\theta = 0)$. For one-dimensional beam-plasma waves

we know that a Fourier analysis with respect to time and space variables is not always convenient for a correct analysis of the convective or absolute character of the instabilities. The well-known correct treatment involves the Laplace transform of the Green's-function formalism.[18-20]

In our case a new difficulty arises from the two-dimensional character of the wave propagation. The standard procedure used in the previously published works[11-14,21] when the beam-plasma system is confined by a cylindrical wave guide with finite transverse radius b, is to expand the solution of the wave propagation in a complete set of radial wave functions, in our case the Bessel function, whose argument is determined by the boundary conditions at the wave-guide radius. This is a correct mathematical approach when the wave reflection at the guide surface establishes for $t \to \infty$ a standing radial wave pattern. Nevertheless, this procedure holds only if the growth rate of instability verifies the inequality $|\mathrm{Im}\omega|_{\max} b < v_{g_\perp}$. In the opposite limit, the guide has no effect on the instability. The unstable solutions, which arise from the injection of a beam of radius $a (a < b)$ along the wave guide are very different from the stable modes. This effect will considerably modify the nonlinear behavior of such instabilities. Consequently, in such a case, we think that our treatment, where we consider the system as an open one, will be more correct. In such a situation, we cannot *a priori* expand the solutions through a set of eigenfunctions convergent at $r \to \infty$, for the radial-wave behavior cannot be prescribed independently of the stability analysis. Let us emphasize this important point some more. Let the solutions of the wave potential be of the form $\Phi \sim \Phi(r) \exp i(k_\parallel z - \omega t)$, outside the beam. Two different kinds of radial behavior may be expected, depending on the value of the real frequency ω. They are as follows:

(a) In the nonpropagative frequency windows, when ω lies between ω_c and ω_p or when ω is greater than ω_H, the propagation is possible only inside the beam, not outside. One expects the wave to remain confined to the beam vicinity, i.e., in a WKB analysis, $\Phi \sim \exp(+i \int k_r dr)$, with $\mathrm{Im}k_r < 0$ and $|\mathrm{Im}k_r| \gg |\mathrm{Re}k_r|$. For relatively weak instabilities, i.e., for small values of the perturbative parameter $\epsilon = n_b/n_p$, the deformation in the complex $(\omega, k_\parallel)$ planes (necessary for the stability analysis) will not qualitatively modify this radial behavior. Consequently, the radial behavior can be prescribed *a priori*, as in Ref. 3.

(b) In the propagative windows $\omega < \omega_c$ and $\omega_p < \omega < \omega_H$ (where the unstable waves may be radiated out of the beam region) we expect $|\mathrm{Im}k_r| \ll |\mathrm{Re}k_r|$ in the same WKB analysis as before. This behavior implies a radial Green's-function analysis before the exploration of the complex $(\omega, k_\parallel)$ planes. Indeed, one cannot prescribe a normal-mode behavior due to the unknown sign of $\mathrm{Im}k_r$; and it is possible to find, as a result of complete analysis, that the solution is radially diverging. This is surprising because outside the beam there is no amplifying medium but, in fact, the explanation is simple and is related to the propagative properties of the magnetized plasma medium. Suppose, for the sake of simplicity, that the spatial and temporal growth rates are sufficiently small to allow the usual expansion procedure of the dispersion equation $D(k_r, k_\parallel, \omega) = 0$ which connects the imaginary part of $k_r, k_\parallel, \omega$ through the perpendicular and parallel group velocities of the waves in the outer medium. We then obtain the approximate relation $\mathrm{Im}k_r \simeq (1/v_{g_\perp}^{\mathrm{out}})(\mathrm{Im}\omega - v_{g_\parallel}^{\mathrm{out}} \mathrm{Im}k_\parallel)$. Inside the beam, the parallel group velocity of the unstable waves $v_{g_\parallel}^{\mathrm{in}}$ is always positive, and due to energetic arguments (no power flow coming from infinity) $v_{g_\perp}^{\mathrm{out}}$ is also positive. When ω lies in the low-frequency window $\omega < \omega_c$, $v_{g_\parallel}^{\mathrm{out}} \sim V_b(\omega_c^2 - \omega^2)/\omega_c^2$ is positive. From the above relation, $\mathrm{Im}k_r$ is also positive (for $\mathrm{Im}\omega > 0$ and/or $\mathrm{Im}k_\parallel < 0$, corresponding to wave instability), and the radial function $\Phi(r)$ is expected to converge at $r \to \infty$. On the contrary, for the high-frequency window $\omega_p < \omega < \omega_H$,

$$v_g^{\mathrm{out}} \sim -V_b \frac{(\omega_H^2 - \omega^2)(\omega^2 - \omega_p^2)}{2\omega_c^2(\omega^2 - \omega_H^2/2)}$$

is negative (when $\omega_c < \omega_p$). When the corresponding instability is convective the spatio-temporal behavior of the solution is essentially given by $|\mathrm{Im}k_{\parallel}|_{\max}$ at $\mathrm{Im}\omega = 0$ [lowering of the Bromwich path down to the $\mathrm{Re}(\omega)$ axis[18]] and $\mathrm{Im}k_r < 0$, giving rise to radial convective behavior. When the instability is absolute, the behavior is given by the $(\mathrm{Im}\omega_0, \mathrm{Im}k_0)$ of the saddle point[18] and the radial-behavior results from a conflict between the modulus of $\mathrm{Im}\omega_0$ and $\mathrm{Im}k_{\parallel 0}$: If $|\mathrm{Im}\omega_0/\mathrm{Im}k_{\parallel 0}| > |v_{g\parallel 0}^{\mathrm{out}}|$ we obtain $\mathrm{Im}k_r > 0$ and a radially convergent solution. In the opposite case, $\mathrm{Im}k_r$ is negative and the observed potential at the given (z, t) position is expected to grow with r, reflecting the spatial growing of the wave along the beam in an apparent radial amplification. Such behavior cannot be obtained by an expansion of the solution in a complete set of radial wave functions and can only be treated by a radial Green's-function analysis. All the situations we have described here may be illustrated by our numerical and analytical analysis (see Sec. III and Appendix C).

In the remainder of this section, we construct the complete Green's function $G(r, r_0, z - z_0, t - t_0)$ of the linearized beam-plasma system of equations. It is well known that such a function would

describe the temporal evolution of a perturbation which is initially localized at $r=r_0$ and $z=z_0$. The $(z-z_0)$ axial dependence is due to the translational invariance of the system along the beam's axis and the $(t-t_0)$ temporal dependence is associated with conservative properties.

After a Fourier transform upon z and a Laplace transform upon time, we get the function $\tilde{G}(r, r_0, k_\parallel, \omega)$:

$$\tilde{G}(r, r_0, k_\parallel, \omega) = \int_{-\infty}^{+\infty} dz \int_0^{+\infty} d\tau\, e^{-i(k_\parallel z - \omega\tau)} G(r, r_0, z, \tau) .$$

The Green's function G may be obtained from $\tilde{G}$ by a complex integration along the Bromwich path:

$$G(r, r_0, z, \tau) = \int_{i\gamma-\infty}^{i\gamma+\infty} d\omega \int_{-\infty}^{+\infty} dk_\parallel \tilde{G}\, e^{i(k_\parallel z - \omega\tau)} ,$$

where γ lies above all the possible singularities of $\tilde{G}(r, r_0, k_\parallel, \omega)$.

For our system, $\tilde{G}$ is the solution to the following differential equation:

$$\frac{1}{r}\frac{\partial}{\partial r}\left(\epsilon_\perp(r) r \frac{\partial}{\partial r}\tilde{G}\right) - k_\parallel^2 \epsilon_\parallel(r)\tilde{G} = A\delta(r-r_0) ,$$

with

$$\begin{aligned} \epsilon_\perp(r) &= Y(a-r)\epsilon_\perp^{in} + Y(r-a)\epsilon_\perp^{out} , \\ \epsilon_\parallel(r) &= Y(a-r)\epsilon_\parallel^{in} + Y(r-a)\epsilon_\parallel^{out} , \end{aligned} \tag{1a}$$

where

$$\epsilon_\perp^{in}(\epsilon) = 1 - \frac{\omega_p^2}{\omega^2-\omega_c^2} - \frac{\epsilon\omega_p^2}{(\omega - k_\parallel v_b)^2 - \omega_c^2} ,$$

$$\epsilon_\parallel^{in}(\epsilon) = 1 - \frac{\omega_p^2}{\omega^2} - \frac{\epsilon\omega_p^2}{(\omega - k_\parallel v_b)^2} ,$$

$$\epsilon_\perp^{out} = \epsilon_\perp^{in}(0) , \quad \epsilon_\parallel^{out} = \epsilon_\parallel^{in}(0) ,$$

and $Y(x)$ is the usual Heaviside's step function. The Green's function $\tilde{G}$ must be continuous and convergent along the Fourier-Laplace inversion path $(\omega, k_\parallel)$ and satisfy the connection condition (see Appendix A):

$$\epsilon_\perp^{out}\frac{\partial}{\partial r}\tilde{G}(a^+, r_0, k_\parallel, \omega) - \epsilon_\perp^{in}\frac{\partial}{\partial r}\tilde{G}(a^-, r_0, k_\parallel, \omega) = \begin{cases} 0 \text{ if } a \neq r_0 \\ A \text{ if } a = r_0 \end{cases} . \tag{1b}$$

As shown in Appendix A, where Eqs. (1a) and (1b) are solved, the radial dependence of the transformed Green's function for $r > \sup[r_0, a]$ is given by $\tilde{G} \sim H_0^{(1)}(K_\perp^{out} r)$ or $H_0^{(2)}(K_\perp^{out} r)$, where

$$K_\perp^{out} = k_\parallel (\epsilon_\parallel^{out}/\epsilon_\perp^{out})^{1/2} = k_\parallel \left(\frac{\omega^2-\omega_p^2}{\omega^2}\frac{\omega^2-\omega_c^2}{\omega^2-\omega_H^2}\right)^{1/2}$$

and $H_0^{(1)}, H_0^{(2)}$ are Hankel functions.[22] The choice of the correct Green's function is related to the radial convergence of the solution when $r \to +\infty$ as $(k_\parallel, \omega)$ lies on the inversion path.

It is also shown in Appendix A that the "good choice" is

$$\tilde{G} \sim H_0^{(1)}\left[ik_\parallel r\left(+\frac{\omega^2-\omega_p^2}{\omega^2}\frac{\omega^2-\omega_c^2}{\omega^2-\omega_H^2}\right)^{1/2}\right],$$

with the usual branch cut for the square-root function (on the real negative axis). Then, the dispersion equation is simply the equation which gives the singularities of the Green's function in the $(\omega, k_\parallel)$ planes.[18] With the normalized variables $\alpha = \omega/\omega_p$, $z = k_\parallel V_b/\omega_p$, $\alpha_c = \omega_c/\omega_p$, $\alpha_H = \omega_H/\omega_p$, and $S = \omega_p a/V_b$ this dispersion relation reads

$$T\frac{J_1(T)}{J_0(T)} = \frac{\epsilon_\perp^{out}}{\epsilon_\perp^{in}} U\frac{H_1^{(1)}(U)}{H_0^{(1)}(U)} , \tag{2a}$$

$$S^2 z^2 \epsilon_\parallel^{in} + T^2 \epsilon_\perp^{in} = 0 , \tag{2b}$$

$$S^2 z^2 \epsilon_\parallel^{out} + U^2 \epsilon_\perp^{out} = 0 . \tag{2c}$$

Let us now, using previous formulas, explain the connection between our result and the result obtained previously in a system with a wave guide of radius b (Eq. 11 of Ref. 11). To simplify the algebra, we take the limit of plane geometry and obtain, respectively,

$$T\tan T = -iU\epsilon_\perp^{out}/\epsilon_\perp^{in} , \tag{3a}$$

$$T\tan T = -iU\frac{\epsilon_\perp^{out}}{\epsilon_\perp^{in}}\frac{e^{iU(1-b/a)} + e^{-iU(1-b/a)}}{e^{iU(1-b/a)} - e^{-iU(1-b/a)}} , \tag{3b}$$

using the previous definition for the variables T and U. These two dispersion relations are completely different for real ω: The right-hand side of Eq. (3a) is purely imaginary when that of Eq. (3b) is real. Hence, the limit $b \to \infty$ of the dispersion equation (3b) cannot give our result in that case. Nevertheless, the two dispersion equations become identical, if we first make $\mathrm{Im}\,\omega > 0$ and then take the limit $b \to \infty$. This last identification is necessary because in that case the instability does not depend on the reflection at the wall: This is only approximately correct if $\mathrm{Im}(k_r b) \gg 1$ (or $b\,|\mathrm{Im}\,\omega| \gg v_{e_\perp}$), when the potential of the wave is strongly attenuated at the guide radius b.

II. LOW-FREQUENCY INSTABILITIES ($\omega < \omega_c$)

In the lowest-frequency range ($\omega < \omega_c$) we are dealing with radiated beam-plasma waves ($|\mathrm{Im}k_r| \ll |\mathrm{Re}k_r|$) which have been found previously.[9] We expect the unstable waves to have the following

feature: For real k_z and complex ω the sign of the parallel group velocity $\partial\omega/\partial k_{\parallel} > 0$ implies that the waves have a radial mode structure (i.e., they converge for $r \to +\infty$).

In principle, we have to follow the singularities of the Green's function by a classical deformation in the complex Laplace plane (ω, k_z) from (complex ω, real k_z) to (real ω, complex k_z). We have made a complete numerical study of the Laplace transform of the Green's function. The operating scheme of the numerical analysis will be described latter (Sec. IIIC). As expected from previous remarks we have only found convectively unstable waves: they remain radiated in the radial direction in the sense that $\mathrm{Re}k_{\perp}^{\mathrm{out}} > \mathrm{Im}k_{\perp}^{\mathrm{out}}$ and are convectively amplified along the beam axis. In this section we complete both analytically and numerically the published results.[9] We consider successively the cyclotronic and Cerenkov modes $\omega \simeq k_{\parallel}V_b + \omega_c$ and $\omega \simeq k_{\parallel}V_b$. We compare the spatial growths of the two kinds of instabilities for different values of the beam and plasma parameters and different radial wave structures (characterized by the number of nodes of the electric wave potential inside the beam).

A. Cyclotronic modes

It is convenient to introduce a small, dimensionless variable $\chi = z - \alpha - \eta\alpha_c$ ($\eta = \pm 1$, respectively, for the slow and fast cyclotronic waves). Taking into account the conditions of geomagnetic experiments ($\alpha_c^2 \ll 1$, $\epsilon \ll 1$) and of weak instability ($|\chi| < \alpha_c/2$) we may easily simplify our system of equations (2):

$$\frac{1}{T}\frac{J_1(T)}{J_0(T)} \simeq \frac{1}{U}\frac{H_1^{(1)}(U)}{H_0^{(1)}(U)},$$

$$U^2 \simeq -S^2\frac{z^2}{\alpha^2}(\alpha^2 - \alpha_c^2), \tag{4}$$

$$T^2 \simeq -S^2\frac{z^2}{\alpha^2}(\alpha^2 - \alpha_c^2)\frac{2\eta\alpha_c\chi}{2\eta\alpha_c\chi + \epsilon(\alpha^2 - \alpha_c^2)}.$$

The dispersion relation is solved analytically with good accuracy only for large or small values of U. For cyclotronic modes $z \sim \alpha_c(1 + \eta\alpha_c/\alpha)$ and $U \sim S(1 + \eta\alpha_c/\alpha)(\alpha_c^2 - \alpha^2)^{1/2}$. For a thick beam ($S\alpha_c \gg 1$), U is large in the whole frequency range, except in the close vicinity of the cyclotronic frequency. For a thin beam ($S\alpha_c \ll 1$), U is large for small frequencies ($\alpha < S\alpha_c^2$), i.e., $\omega < \omega_c^2 r_0/V_b$. We may take for large values of U the asymptotic expansion of the Hankel functions and obtain

$$T \simeq j_{1,n} + i/U, \tag{5}$$

where $j_{1,n}$ is the nth zero of the Bessel function $J_1(x)$ for $n \geq 1$. An approximate solution of the dispersion relation is now given by

$$z \simeq \eta\alpha_c + \alpha - \eta\frac{\epsilon}{2\alpha_c}y,$$

$$y \simeq (j_{1,n}/U)^2(\alpha_c^2 - \alpha^2)(1 + 2i/Uj_{1,n}) \times [1 - (j_{1,n}/U)^2(1 + 2i/Uj_{1,n})]^{-1}, \tag{6}$$

$$U \simeq S(1 + \eta\alpha_c/\alpha)(\alpha_c^2 - \alpha^2)^{1/2}.$$

We verify with Eq. (6) the standard result; the only unstable cyclotronic mode is the slow mode $\mathrm{Im}z < 0$ for $\eta = 1$. $\mathrm{Im}z$ (like $\mathrm{Im}z/\mathrm{Re}z \sim \mathrm{Im}z/\alpha_c$) grows at first like α^3. For a thin beam ($S\alpha_c \ll 1$) the spatial growth rate is maximum ($\mathrm{Im}z|_{\max} \sim \epsilon\alpha_c j_{1,n}^2/4$) for α close to $S\alpha_c^2/j_{1,n}$ ($\omega/\omega_c \sim \omega_c r_0/V_f$), when for thick beams, it grows up to frequencies very close to α_c where the previous formulas break.

In the close vicinity of the cyclotronic frequency, we take $U \sim 2S(\alpha_c^2 - \alpha^2)^{1/2} \to 0$ for the slow mode, use the expansion of the Hankel functions for small argument and obtain

$$T \simeq j_{0,n} + \frac{4S^2(\alpha_c^2 - \alpha^2)}{j_{0,n}}\left(\ln[2e\gamma(\alpha_c^2 - \alpha^2)^{1/2}] + \frac{i\pi}{2}\right),$$
$$z \simeq 2\alpha_c - \frac{\epsilon(j_{0,n})^2}{8S^2\alpha_c} - \frac{i\pi}{2}\frac{\epsilon}{\alpha_c}(\alpha_c^2 - \alpha^2). \tag{7}$$

$j_{0,n}$ is the nth zero of $J_0(x)$ and γ is the Euler constant.

B. Cherenkov modes

To limit the somewhat cumbersome algebra we restrict our analytical treatment to the thin-beam case ($S\alpha_c \ll 1$). We easily deduce from Eq. (2) the following approximate dispersion relation:

$$\frac{TJ_1(T)}{J_0(T)} = -\frac{\alpha^2 - \alpha_H^2}{(1 + \epsilon/\alpha_c^2)(\alpha^2 - \alpha_1^2)}\ (\ln U/2 - i\pi/2)^{-1},$$
$$T^2 = -S^2\alpha^2\left(1 - \frac{1}{\alpha^2} - \frac{\epsilon}{(z - \alpha)^2}\right)\frac{\alpha^2 - \alpha_c^2}{(1 + \epsilon/\alpha_c^2)(\alpha^2 - \alpha_1^2)}, \tag{8}$$

with $\alpha_1 = \alpha_c[1 + 1/(\epsilon + \alpha_c^2)]^{1/2}$.

For a weak instability we expect $z \sim \alpha$ and $U \sim S(\alpha_c^2 - \alpha^2)^{1/2}$ to be small compared with unity. We may expand Eq. (8) in the vicinity of $TJ_1(T) \simeq 0$. If we take $T \simeq j_{1,n}$ we obtain a negligible growth rate. The fastest growing mode has a wave potential with a zero node inside the beam ($T \simeq 0$):

$$\frac{T^2}{2} \simeq \frac{\alpha^2 - \alpha_H^2}{(1 + \epsilon/\alpha_c^2)(\alpha^2 - \alpha_c^2)}\left(\ln\frac{U}{2} + \frac{i\pi}{2}\right)^{-1},$$
$$z \simeq \alpha - \alpha S\left(\frac{\epsilon(\alpha_c^2 - \alpha^2)}{2(\alpha_H^2 - \alpha^2)}\right)^{1/2} \times\left[\ln\frac{Se^{\gamma}}{2}\left(\frac{(1 - \alpha^2)(\alpha_c^2 - \alpha^2)}{\alpha_H^2 - \alpha^2}\right)^{1/2} + \frac{i\pi}{2}\right]^{1/2}. \tag{9}$$

We verify later on the numerical results that are in agreement with Eq. (9), that $|\mathrm{Im}z|$ is maximum

for $\alpha \sim \alpha_c/\sqrt{2}$ and vanishes when $\alpha \to \alpha_c$.

From our analytical results [Eqs. (6), (7), and (9)] we verify our initial assertion: The dispersion relation is essentially real and, in this frequency window, follows the cold-plasma dispersion relation. The beam has nevertheless two effects; it removes the degeneracy of the cold-plasma dispersion in infinite medium and quantizes the radial wave number, and it drives the instability. In the dispersion relation for the beam-plasma system the spatial growth rate follows from the radiative character of the wave, that is to say it arises from the imaginary part of the function UH_1^1/H_0^1 for real values of U. Let us now give our numerical results to confirm and extend the analytical formulas.

C. Influence of the beam parameters on the unstable modes

As shown by Eqs. (6), (7), and (9), Imz is essentially proportional to the beam density (parameter ϵ), for the cyclotronic mode and to $S\sqrt{\epsilon}(\omega_{pb} \times r_0/V_b)$ for the Cherenkov mode. Hence, for a given injection experiment, where $S\sqrt{\epsilon}$ is fixed ($S^2\epsilon \simeq 3 \times 10^4 I/V^{3/2}$, with I in amperes, the injection current, and V in volts, the injection voltage), as well as the local parameters of the ionospheric plasma (ω_p and ω_c, hence α_c), the Cherenkov instability is quite insensitive to the beam radius, when the cyclotronic one is more intense for thin or dense beams and takes place essentially at a very low frequency (say $\alpha \sim S\alpha_c^2$ or $\omega/\omega_c \sim r_0\omega_c/V_b j_{1,n}$).

Figure 7 shows the evolution of the relative spatial growth rate (Im$k_\parallel$/Re$k_\parallel$) for a realistic injection situation [$S^2\epsilon \simeq 10^{-2}$ for $I = 1.7$ A (0.6 A); $V = 30$ keV (15 keV); $\omega_c/\omega_p = 0.4$] and different values of the beam parameters ($\epsilon = \alpha_c^2/2$; $\epsilon = \alpha_c^2/20$; $\epsilon = \alpha_c^2/200$). We choose the zero-node Cherenkov instability and the one-node cyclotronic instability. From the numerical results we obtain the lengths of exponentiation, for the cyclotronic and Cherenkov modes $L_{c_y} \simeq (V_b/\omega_c)(\text{Im}z/\text{Re}z)_{\max}$ and $L_c = [1/(\text{Im}z)_{\max}]V_b/\omega_p$. They may be very different for the two unstable branches and are quite sensitive to the beam's parameter ϵ. For the first case, $(\epsilon = \alpha_c^2/2 = 0.08) L_c \simeq 8L_{c_y}$, while for the second one, $(\epsilon = \alpha_c^2/20 = 0.008) L_c \simeq 0.6 L_{c_y}$.

D. Influence of the radial structure of the modes

For modes with a higher number of internal nodes, the numerical computation shows that the Cherenkov instabilities are much weaker. In the case of Fig. 8, $(\text{Im}z/\text{Re}z)_{\max}$ is two orders of magnitude smaller for the one-node wave than for the zero-node wave. On the contrary, the relative

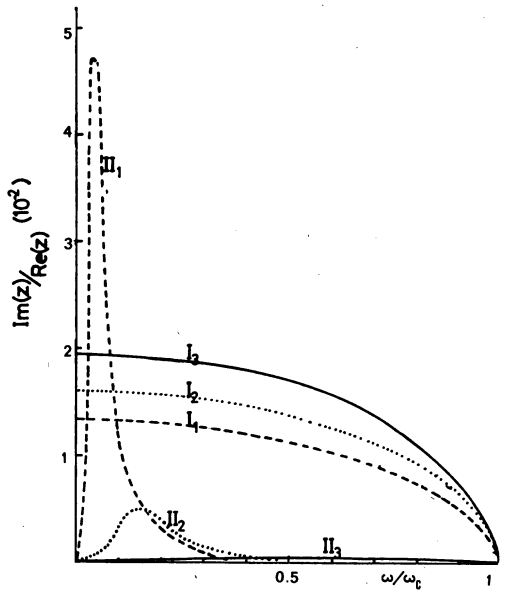

FIG. 7. Influence of the beam's electronic density on the relative spatial growth rate (RSGR) of the low-frequency instabilities: I and II stand for Cherenkov and cyclotronic branches, respectively. Indexes (1, 2, 3) refer to the three values ϵ/α_c^2 (1/2, 1/20, 1/200).

spatial growth rate of the cyclotronic instability has a larger maximum, which occurs for lower frequencies ($\alpha \sim S\alpha_c^2/j_{1,n}$), (see Fig. 8), when the number of internal nodes increases.

E. Influence of the plasma parameters

The only important parameter is $\alpha_c = \omega_c/\omega_p$. The cyclotronic mode is enhanced by a decrease

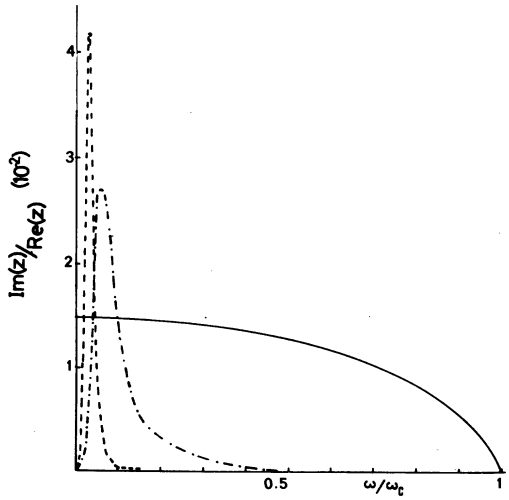

FIG. 8. Influence of the nodes number on the RSGR: ------ two-node cyclotron wave, –·– one-node cyclotron wave, —— zero-node Cherenkov wave, $\epsilon = \alpha_c^2 = 4 \times 10^{-2}$, $S = 1$. With the same parameters the RSGR for the one-node Cherenkov wave is about 10^{-4}.

of the relative gyrofrequency; $(\mathrm{Im}z/\mathrm{Re}z)_{\max}$ occurs for $\omega/\omega_c \sim S\alpha_c/j_{1,n}$ which grows with α_c (Fig. 9). On the contrary, the zero-node Cherenkov-type instability increases with the relative gyrofrequency (see Fig. 10).

III. THE HIGH-FREQUENCY RANGE ($\omega_c < \omega < \omega_H$)

We limit our investigation to the range of frequencies $\omega_c < \omega < \omega_H$. As demonstrated in Appendix B, the waves are stable in the upper-frequency range ($\omega > \omega_H$). In contrast with the low-frequency range, where the instabilities are weak and convective, the complex mapping $k(\omega)$ for real values of the frequency greater than ω_c, has double roots and even saddle points outlining the presence of absolute instabilities. These singularities occur in the $[\omega_p, \omega_H]$ propagative range where the negative group velocity of the plasma waves may induce, by coupling with the Cherenkov and cyclotronic beam's waves, a backward-wave mechanism.

As we have already mentioned in the Introduction, we classify the solutions of (2), when the real part of the normalized frequency α varies from α_c to α_H, by the number of their internal nodes. The real part of $T(\alpha)$ remains bounded by two consecutive zeros of $J_1(x)$, $j_{1,l}$, and $j_{1,l+1}$, and the number of nodes (or zeros of the real part of the associated potential) for a transverse variable r below the beam's radius a, are consequently l or $l+1$, depending on the position of $\mathrm{Re}[T(\alpha)]$ with respect to the lth zero of $J_0(x)$ ($j_{1,l} < j_{0,l} < j_{1,l+1}$).

This corresponds to following simultaneously the different branches of the dispersion equation which belong to the same sheet of the Riemann surface associated with the $k_{\parallel}(\omega)$ mapping [or the $z(\alpha)$ mapping]. On each of these sheets we distinguish a "normal" and a cyclotronic branch, which connect continuously, for $\mathrm{Re}(\alpha) < \alpha_c$, with the Cherenkov and the cyclotronic waves (respectively) met previously in the low-frequency region. In addition, there is also a "surface" branch (for zero- or one- node sheets) which is characterized by the fact that for a certain value of the real normalized frequency $\{\alpha_1 = \alpha_c[1 + 1/(\epsilon + \alpha_c^2)]^{1/2}\}$ the imaginary part of the function $T(\alpha)$ diverges, giving rise to a surface wave and an essential branch characterized by the divergence of the complex function $z(\alpha)$ at the plasma frequency ($\alpha = 1$).

In Sec. IIIA we shall give the analytical expression of $z(\alpha)$ for α real, and low values of the beam's plasma parameter (weak-beam approximation and/or low normalized gyrofrequency α_c) which allows a simplification of the dispersion relation. In the second part we present systematic results of the numerical investigation, with realistic parameters for an ionospheric injection experiment.

A. Analytical results

In this section we obtain partial analytical results. Our formulas do not describe the whole mapping of $z(\alpha)$ which is necessary to understand the convective or absolute character of the various instabilities, or to follow the radial behavior of the Green's function. These results are in fact obtained by the expansion of our system of equations in terms of small parameters, or in the vicinity of some frequencies. Nevertheless the analytical formulas are useful to classify systematically the branches of the dispersion relation and allow an interpretation of the numerical results. In Appendix C, we take a complementary point of view and compute the analytical condition for absolute (convective) instability in the upper-frequency window. In the following, we treat separately the cyclotronic branch and the other branches of the dispersion relation.

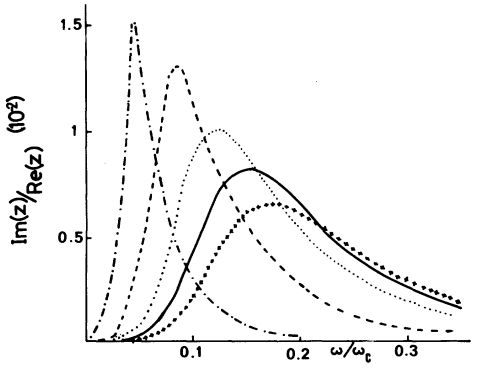

FIG. 9. Influence of α_c on the RSGR of cyclotronic one-node wave ($S^2\epsilon = 10^{-2}$, $\epsilon = 2\times10^{-2}$): $-\cdot-$ $\alpha_c = 0.2$; ---- $\alpha_c = 0.4$; $\cdots$ $\alpha_c = 0.6$, —— $\alpha_c = 0.8$, + + + $\alpha_c = 1$.

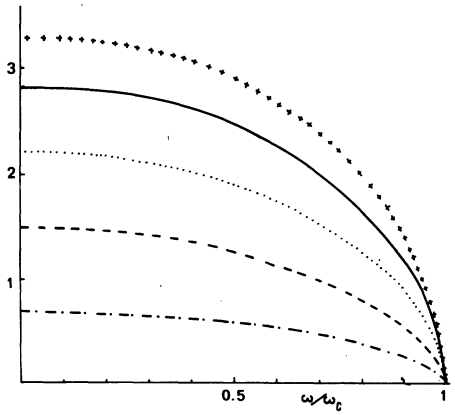

FIG. 10. Influence of α_c on the RSGR of the Cherenkov zero-node wave (same notation as Fig. 9).

1. The cyclotronic branch

As in Sec. II A, we assume a weak deviation from the cyclotronic resonance line ($\omega - kv_b + \eta\omega_c$ where $\eta = \pm 1$), and introduce the small dimensionless parameter χ defined by $\chi = z - \alpha - \eta\alpha_c$. To the most significant order in χ the dispersion equation (2) may then be written

$$U^2 = -S^2\left(1+\eta\frac{\alpha_c}{\alpha}\right)^2 \frac{(\alpha^2-1)(\alpha^2-\alpha_c^2)}{(\alpha^2-\alpha_H^2)}, \tag{10a}$$

$$T^2 = -S^2\left(1+\eta\frac{\alpha_c}{\alpha}\right)^2\left(1-\frac{\epsilon}{\alpha_c^2}\right)(\alpha^2-\alpha_2^2) \times \frac{2\eta\alpha_c\chi(\alpha^2-\alpha_c^2)}{2\eta\alpha_c\chi(\alpha^2-\alpha_H^2)-\epsilon(\alpha^2-\alpha_c^2)}, \tag{10b}$$

$$\frac{1}{T}\frac{J_1(T)}{J_0(T)} = \frac{1}{U}\frac{H_1^{(1)}(U)}{H_0^{(1)}(U)}\frac{\alpha^2-1}{(1-\epsilon/\alpha_c^2)(\alpha^2-\alpha_2^2)}, \tag{10c}$$

where the characteristic frequency α_2 is given by $\alpha_2^2 = 1/(1-\epsilon/\alpha_c^2)$.

For a real α between α_c and 1, we see from (10a) that U is purely imaginary; the right-hand side of (10c) is consequently purely real as T, and from (10b) we conclude that χ is real. Nevertheless, due to an intricate behavior of the $K_{\parallel}(\omega)$ mapping [see Fig. 3(c)] the cyclotronic branch becomes unstable for $\alpha \gtrsim \alpha_1$. In the propagative range $[1, \alpha_H]$, χ has an imaginary part. Assuming a thin and dilute beam ($\alpha_c S \ll 1$ and $\epsilon \ll \alpha_c^4$), choosing the real frequency outside the close vicinity of 1 and α_H $(1-\epsilon/\alpha_c^2)^{-1/2} \ll \alpha \ll \alpha_H - S^2\alpha_c^2/2\alpha_H$, the right-hand side of (10c) is large and T is of the order $j_{0,n}$ [$j_{0,n}$ is the nth zero of $J_0(x)$]. Then we obtain the following approximate formulas:

$$\chi = \eta\frac{\epsilon}{2\alpha_c}\frac{(\alpha^2-\alpha_c^2)A}{(\alpha^2-\alpha_c^2)+(\alpha^2-\alpha_H^2)A}, \qquad A \simeq \frac{1}{S^2}\left(\frac{j_{0,n}^2}{\alpha_2^2-\alpha^2} - \frac{2U}{(\alpha^2-1)}\frac{H_0^{(1)}(U)}{H_1^{(1)}(U)}\right), \tag{11}$$

with U given by (10a). The results are similar to the lowest-frequency range ($\alpha < \alpha_c$): The imaginary part of χ is directly related to the radiating wave behavior outside the beam [$\mathrm{Im}\chi$ comes from $\mathrm{Im}(A)$, i.e., $\mathrm{Im}H_0^{(1)}(H_1^{(1)})$]. $\mathrm{Im}\chi$ vanishes for $\alpha \to \alpha_H$ and has a maximum value for an intermediate frequency. If a cyclotronic mode is convectively unstable along the magnetic field, simultaneously the potential becomes divergent outside the beam, as follows from the relationship between U and z. In (10a), χ has been neglected in comparison with 1; taking this correction into account one finds $\mathrm{Im}(U) < 0$ for $\mathrm{Im}\chi < 0$, and $\mathrm{Re}(U) > 0$.

We already pointed out in part I that $\mathrm{Im}k_{\perp}^{\mathrm{out}} \simeq -\mathrm{Im}k_{\parallel}v_{g_{\parallel}}/v_{g_{\perp}}$. Then in the frequency range $1 < \alpha < \alpha_H$, $v_{g_{\parallel}} < 0$ and $v_{g_{\perp}} > 0$ outside the beam [the energy has to flow from the beam, a condition equivalent to $\mathrm{Re}(U) > 0$] and $\mathrm{Im}k_r < 0$. The wave potential seems to be divergent outside the beam for a convectively amplified mode. Formulas (2) have been integrated numerically and the results for the maximum value of $\mathrm{Im}z$ are given in Tables I(a) and I(b) for different values of ϵ, and α_c; ϵS^2 has the constant value $\epsilon S^2 = 10^{-2}$. These partial results show an enhancement (for values with an asterisk) of the spatial growth rate of the cyclotronic instability for certain values of the parameters α_c and ϵ. In Sec. III B such an enhancement will be explained by the mutual influence of three different branches of the dispersion relation: A secondary saddle point which involves the cyclotronic branch is created by attraction of a double root by an existing primary saddle point. For these values of the beam and plasma parameters, the cyclotronic branch participates in a nonconvective instability.

2. The other branches

To explore the other branches of the dispersion relation analytically, we still restrict ourself to a thin beam ($S\alpha_c \ll 1$) and small gyrofrequencies ($\alpha_c \ll 1$). Assuming a Cherenkov resonance ($z \simeq \alpha$ or $\omega \simeq k_{\parallel}V_b$) we see that the right-hand side of the dispersion equation (2a) has to be small, except in the vicinity of the characteristic frequency $\alpha_1 = \alpha_c(1+1/\alpha_c^2+\epsilon)^{1/2}$ where ϵ_1^{in} must have a zero (for $z \simeq \alpha$). If $\epsilon < \alpha_c^4$, $\alpha_1 \sim \alpha_H$ is no longer a characteristic frequency. If $\alpha_c^4 < \epsilon \lesssim \alpha_c^2\alpha_1 \lesssim 1$, α_1 matters for a discussion of the Cherenkov mode. In this case, for $\alpha \neq \alpha_1$, we shall look for solutions with $|T| \simeq 0$ or $|T| \simeq j_{1,n}$ [nth zero of the Bessel function $J_1(x)$] which are the values of T that minimize the left-hand side of (2a), when, for $\alpha \simeq \alpha_1$ we shall look for solutions with $|T| \simeq \infty$ or $|T| \simeq j_{0,n}$ [nth zero of $J_0(x)$].

TABLE I. Variation of the maximum value of $\mathrm{Im}z$ for $1 < \alpha < \alpha_H$ on the cyclotronic branch.

α_c \ ϵ	10^{-1}	10^{-2}	10^{-3}
(a) Corresponds to the zero- or one-node sheet $(0 < T < j_{1,1})$.			
0.2	4×10^{-6}	3.4×10^{-4}	10^{-2}
0.4	2×10^{-4}	2.7×10^{-2}	2×10^{-2}
0.6	1.5×10^{-2}	$*10^{-1}$	4.8×10^{-3}
0.8	3×10^{-2}	$*10^{-1}$	1.6×10^{-3}
(b) Corresponds to the one- or two-node sheets $(j_{1,1} < T < j_{1,2})$.			
0.2	6.5×10^{-7}	6×10^{-5}	5.4×10^{-3}
0.4	3×10^{-5}	1.16×10^{-2}	$*8.5\times10^{-2}$
0.6	5.4×10^{-3}	9×10^{-3}	1.7×10^{-2}
0.8	1.12×10^{-2}	$*10^{-1}$	6×10^{-3}

a. Zero node and surface solutions. From (2), assuming $T^2 \ll 1$, we obtain

$$1-\frac{1}{\alpha^2}-\frac{\epsilon}{(z-\alpha)^2}\left(1-\frac{2}{U}\frac{H_1^{(1)}(U)}{H_0^1(U)}\right)^{-1}=0, \qquad (12)$$

where U is given by (2c). For a thin beam and parameter values which allow a close vicinity of the Cherenkov resonance, we compute z easily:

$$z\simeq\alpha\left\{1\pm i\frac{S\sqrt{\epsilon}}{2}\left(\frac{\alpha^2-\alpha_c^2}{\alpha H^2-\alpha^2}\right)^{1/2}\times\left[-\ln\left(\frac{S}{2}\frac{[(1-\alpha^2)(\alpha^2-\alpha_c^2)]^{1/2}}{(\alpha_H^2-\alpha^2)}e^{\gamma}\right)\right]^{1/2}\right\} \qquad (13)$$

(where γ is the Euler constant), together with

$$T\simeq\sqrt{2}\left(\frac{\alpha_H^2-\alpha^2}{(\alpha_1^2-\alpha^2)(1+\epsilon/\alpha_c^2)}\right)^{1/2}\times\left(-\ln\frac{S}{2}\frac{[(1-\alpha^2)(\alpha^2-\alpha_c^2)]^{1/2}}{(\alpha_H^2-\alpha^2)}e^{\gamma}\right)^{-1/2}. \qquad (14)$$

In the range of frequencies $\alpha_c<\alpha<1$, if $\alpha_1>1$, or $\alpha_c<\alpha<\alpha_1$ in the opposite case, the previous formulas show an unstable convective behavior for a body mode (T being essentially real and U imaginary). These formulas are not valid for $\alpha\simeq\alpha_1$ (divergence of T) and also for $\alpha=1$ (divergence of z). Let us now consider successively these two cases.

(i) For $\alpha\simeq\alpha_1$ our exact numerical solution indicates that now $T\simeq j_{0,1}$ (first zero of J_0). By expansions of the system (2) in the vicinity of this value we obtain

$$z\simeq\alpha-i\left(\frac{S\alpha_1}{j_{0,1}}\right)^{1/2}\alpha_c\left(1-\frac{(\alpha_c^2+\epsilon)^2}{2\epsilon}\frac{j_{0,1}}{S\alpha_c^2\alpha_1}(\alpha_1^2-\alpha^2)\right), \qquad (15)$$

and the zero- or one-node branch remains unstable when α goes through the value α_1, contrary to published results.[3] Radially the unstable wave has a mode structure (if $\alpha_1<1$) and is convectively amplified if $\alpha_1>1$ (in this case U is mainly real and positive and has a small negative imaginary part).

In addition to this zero- or one-node branch, a new branch becomes unstable when α crosses the value α_1. T is still given by (2b) and becomes divergent: T is imaginary for $\alpha\sim\alpha_1<1$ and complex for $\alpha_1>1$, the wave has in both cases a surface structure inside the beam. Assuming $|T|\gg1$ and $\alpha\sim\alpha_1$ we obtain

$$z\simeq\alpha-i\frac{\alpha_c^2+\epsilon}{\sqrt{\epsilon}}(\alpha^2-\alpha_1^2)^{1/2}(1+A^{-2})^{-1/2},\qquad A=S\alpha_c\alpha_1\ln\left(\frac{S}{2}e^{\gamma}\frac{[(1-\alpha_1^2)(\alpha_1^2-\alpha_c^2)]^{1/2}}{(\alpha_H^2-\alpha_1^2)}\right). \qquad (16)$$

(ii) For $\alpha\simeq1$, we also have two possibilities. One branch shows a logarithmic decrease of z when α approaches 1, due to the behavior of the Hankel function $H_0^{(1)}(U)$ when U becomes small:

$$z\simeq\frac{2\alpha_c}{S\sqrt{\epsilon}}\frac{1}{(-\ln x)^{1/2}}e^{-i\pi/2}[1-1/\ln(-x/\ln x)], \qquad (17)$$

with

$$x=\frac{e^2\gamma}{\epsilon}(1-\alpha^2),$$

Another branch shows an "essential" behavior ($|z|\to\infty$ when $\alpha\to1$). From (12) we obtain z as a function of α,

$$z\simeq\frac{\alpha_c}{S}\frac{U_0}{(\alpha^2-1)^{1/2}}, \qquad (18)$$

where U_0 is complex and may be easily computed from (12).

b. Solutions with many nodes. Assuming $T\simeq j_{1,n}$ for $\alpha\neq\alpha_1$ the dispersion relation reads [from (2a)]

$$\left(1-\frac{1}{\alpha^2}-\frac{\epsilon}{(z-\alpha)^2}\right)+\frac{j_{1,n}^2}{S^2z^2}\left(\frac{\alpha^2-\alpha_1^2}{\alpha^2-\alpha_c^2}\right)=0 \qquad (19)$$

and with $z-\alpha\simeq0$:

$$z\simeq\alpha\left\{1-i\sqrt{\epsilon}\left[(1-\alpha^2)+\frac{\alpha_1^2-\alpha^2}{\alpha^2-\alpha_c^2}\left(\frac{j_{1,n}}{S}\right)^2\right]^{-1/2}\right\}. \qquad (20)$$

For $\alpha\to\alpha_1$, $T\sim j_{0,n+1}$ and the formula for z is obtained from the zero- one-node result (15) with the substitution $j_{0,1}\to j_{0,n+1}$. For $\alpha\to1$ there is also an essential branch with a similar result for z. In this section, we have not considered the vicinity of the upper hybrid frequency. This is in fact the most interesting domain of frequency where the instabilities may become absolute as observed on the numerical results and explained in Appendix C.

B. Numerical investigation: Stability analysis and structure of the solution

1. Methodology

In order to perform the stability of the Green's function we use the well-known mathematical criteria of Bers and Briggs (13)–(15). It is then necessary to study the mapping of the ω complex plane into the $k_{\parallel}$ complex plane, which is associated with the solutions $k_{\parallel}=k(\omega)$ of Eqs. (2a)–(2c) [formally $D(k_{\parallel}(\omega),\omega)=0$].

In our case the Riemann surface of the function $k(\omega)$ has an infinity of (*a priori*) separated sheets; each sheet corresponds to a value of T (the internal radial wave number) localized approximately between two successive zeros of the function $J_1(x)$. In a given sheet, we explore at first, the lines of the complex-z plane which correspond to a real value of the normalized frequency α. Then, such

a solution being chosen in the negative half-plane (Imz negative), we increase the (positive) imaginary part of the frequency α_i (for a constant real part), until the line $z(\alpha_r + i\alpha_i)$ has definitely crossed the real z axis, that is to say, remains in the positive half-plane for a greater value of the imaginary part of the frequency.

When the mapping remains on the same half-plane there is no instability at all. When it crosses the real z axis, but remains conformal (with no branch point), we obtain a simple convective instability. Another situation occurs when different branches of the dispersion equation—here generally belonging to the same "sheet"—may collapse, for some value of the complex frequency α, at points localized in the negative $k_\parallel$ half-plane. A further distinction has to be made, then, between simple double roots, when two branches belong to the same $k_\parallel$ half-plane as the imaginary part of the frequency is increased infinitely, and a real saddle point which arises in the opposite situation. In this second case, we obtain an absolutely unstable wave, as far as the propagation along the field is concerned. At this point we have to pay attention to the radial structure of the solutions obtained with the Green's function. As shown in Appendix A, for ω and $k_\parallel$ localized on the Bromwich path used to invert the Fourier-Laplace transform, the convergence of the Green's function is insured by a correct choice of the determination of the argument of the Hankel function which describes its external ($r \to \infty$) structure. Nevertheless, in lowering the Laplace path (in the frequency complex plane) up to the real frequency axis, in conformity to the Bers and Briggs procedure, it may happen (and it happens effectively, in our case) that for a certain real frequency range, the sign of the imaginary part of the argument of the Hankel function $k_\perp^{\text{out}} = k_\parallel(\omega)(\epsilon_\parallel^{\text{out}}/\epsilon_\perp^{\text{out}})^{1/2}$ [or $U(\alpha)$ in normalized variable] changes. In this case, the solution is no more a normal mode: it has a convective behavior outside the beam, as already pointed out in Sec. I B.

2. *Numerical operating scheme*

To solve Eqs. (2) we use a computer program based on an iterative Müller's method with deflation.[23] We first choose a value for the real part of the normalized frequency α_r. As we are interested, *a priori*, in waves which grow along the beam ($+z$ direction) we look for solutions $z(\alpha_r)$ which have a negative imaginary part. The imaginary part of the frequency is then increased, until the solution eventually crosses the real z axis. The essential numerical difficulty is to remain on the same branch of the dispersion equation when the complex frequency α is changed. For each value of the complex frequency α, a guessed value of T (say T_0) is assumed (for example, near the analytical values $j_{0,n}$ or $j_{1,n}$), from which the polynomial which relies on z to T and α, [(2b)] is solved. From these eight roots $z_i(\alpha, T_0)$, we retain only the root which minimizes the "distance" of the solution to a given resonance line ($|z-\alpha|$ for Cherenkov modes and $|z-\alpha+\alpha_c|$ for cyclotronic modes), or to an already computed value of z in the same branch. With that root the value of the complex function

$$F_\alpha(T_0) = \epsilon_\perp^{\text{in}} T_0 J_1(T_0) H_0^{(1)}(U) - \epsilon_\perp^{\text{out}} U J_0(T_0) H_1^{(1)}(U),$$

is then computed. Müller's method is then used to solve (with an *a priori* given precision) the equation $F_\alpha(T) = 0$, which gives the expected value of $z(\alpha)$ through the preceding procedure.

3. *Numerical results*

The plasma parameter $\alpha_c(\omega_c/\omega_p)$ and the beam's parameter (total current I and electron energy E) are fixed at values which are relevant for an active ionospheric experiments[1,2] [$\alpha_c = 0.4$; $I = 1.7$ A (0.6A); $E = 30$ keV (15 keV)]. The dimensionless parameter ϵS^2 [$\sim 3\times 10^4 I/(E)^{3/2}$] then keeps the constant value 10^{-2}. We look for three values of the parameter ϵ (8×10^{-2}, 8×10^{-3}, and 8×10^{-4}) which correspond, respectively, to $\alpha_c^2/2$ (Brillouin radius), $\alpha_c^2/20$, and $\alpha_c^2/200$. Such a choice is likely to be suitable for the study of active experiment, where the electron gun's characteristics are definitively fixed. As the angle of injection, with respect to the magnetic-field lines, increases, the radius increases simultaneously, and the beam's density decreases.

Let us choose some cases which show the essential features of the dispersion equation. In the case with the higher beam's density, Figs. 3(a), 3(b) and 3(c) show the characteristics of the (zero- or one-) node Riemann sheet of the dispersion equation. From the (real z or complex α) picture of Fig. 3(a) one sees three unstable branches: Cherenkov branch (I), cyclotronic branch (II), and surface branch (III). Branches II and III appear to be unstable only for $\alpha > \alpha_1 \{\alpha_c[1 + 1/(\epsilon + \alpha_c^2)]^{1/2}\}$. Branches I and II are identified by continuity with their low-frequency properties ($\alpha < \alpha_c$). Figure 3(b) depicts the $z(\alpha)$ mapping into the complex-z plane, for the same Riemannian sheet. As analytically predicted in Appendix C, a saddle point appears through the collapse of the Cherenkov branch with the "essential" branch (IV), at a frequency which is very close to the upper hybrid frequency ($\alpha_H = 1.077$).

In the vicinity of α_1, where for the surface branch (III), $|\mathrm{Im}T/\mathrm{Re}T| \to \infty$, a complex structure of the mapping would appear; Fig. 3(c), which is an enlargement of the small rectangle to the right and above Fig. 3(b), shows that the cyclotronic, Cherenkov, and surface branches are simultaneously connected, at real frequencies close to α_1, through double roots [not saddle points because the $\mathrm{Re}(\alpha) = cte$ lines remain in the same half-plane of the $k_{\parallel}$ complex plane when $\mathrm{Im}(\alpha)$ grows to infinity]. For these beam and plasma parameters the same situation occurs when one looks at a solution with a higher number of nodes. The value of Re (α) where the saddle point occurs becomes closer to the upper hybrid frequency, as predicted by the formulas (C4) of Appendix C.

A comparison between Figs. 3(a) and 11(a), which depict the $-\mathrm{Re}z$ and complex α diagram for the zero- or one-node Riemann sheet, shows that the temporal growth rate of the Cherenkov branch is not significantly affected by a decrease in the beam's density, in agreement with the previous formulas (13), where the imaginary part of this solution is merely a function of the constant parameter ϵS^2. On the contrary, the temporal growth of the cyclotronic instability decreases with ϵ, as predicted by (11). Furthermore, from Fig. 11(b) we observe that the saddle point which connected the branches I and IV in the previous case now disappears. In Appendix C we show that this phenomena is due to an increase in the (negative) imaginary part of the equivalent internal radial wave number; the imaginary part of the (complex) frequency where the saddle point occurs then becomes negative. This fact may be interpreted as a decrease in the reflecting efficiency of the beam's surface as the beam's density decreases. The feedback mechanism which gives rise to the absolute instability becomes consequently insufficient to balance the energy losses radiated out of the beam. With the same beam parameters, as one used for solutions with a higher number of internal nodes, absolute instability is recovered (Figs. 4 and 5). This is consistent with our analytical prediction of Appendix C, where it is shown that the higher the number of nodes, the smaller the critical value of beam density at which the absolute character of the instability disappears.

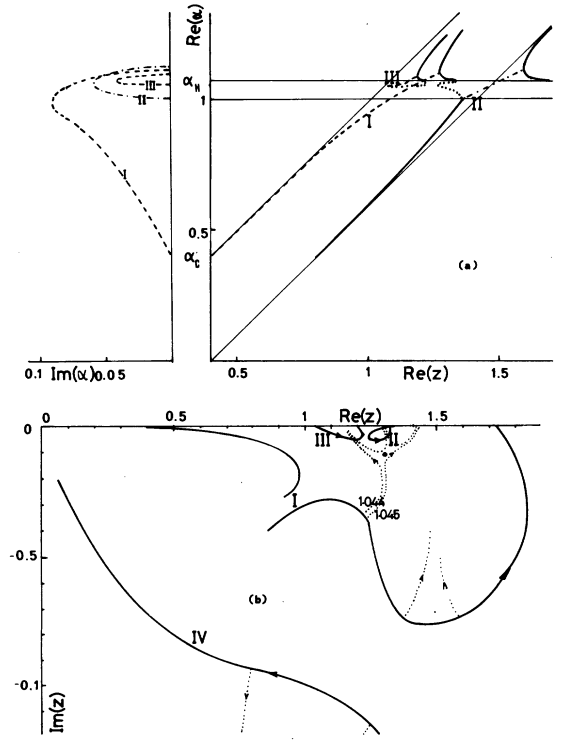

FIG. 11. (a) and (b) The zero-one node sheet for $\epsilon = \alpha_c^2/20$ ($\alpha_c = 0.4$).

As ϵ is further decreased to 8×10^{-4}, the absolute character of the (one- or two-) nodes solutions disappear also. When looking at the (two- or three-) nodes sheet one sees (Fig. 6) another interesting phenomena. As for higher values of ϵ (Figs. 4 and 5) a unique saddle point is observed, together with a simple double root, the three branches I, II, and IV are now connected by two saddle points. This phenomena may be observed for each value of the beam's and plasma's parameter characterized by an enhancement of $\mathrm{Im}z|_{\max}$ for real values of α (see Table I). Such behavior which gives rise to two simultaneous absolute instabilities has already been pointed out in a different physical situation.[24]

In all the cases studied, with beam and plasma parameters relevant to [active ionospheric experiments,[2] the sign of $\mathrm{Im}U$ which corresponds to absolute instability at different saddle points is negative. Hence, as previously pointed out and further discussed in Appendix C [inequalities—(C9)], we are concerned about solutions which are radially amplified wave packets and which present a nonconvective unstable behavior in the beam region only.

CONCLUSION

Our Green's-function formalism allows a simple interpretation of the different electrostatic instabilities produced by a finite, cold, electron beam flowing into a uniform infinite magnetized plasma. These conditions are realistic for active ionospheric electron-beam experiments, such as the ARAKS experiment. Let us summarize our main

results for the different domains of frequencies. In the higher-frequency range ($\omega \sim \omega_b, \omega_H$) we have shown that the most unstable waves occur at a frequency which lies just below the upper hybrid frequency. They may become absolute, when the reflecting efficiency of the beam's boundary is sufficient to limit power losses by outward radiation and consequently to allow a feedback mechanism to take place in the active region. We have analytically determined and numerically verified the beam's density threshold corresponding to that energy balance. This effect, which is quite sensitive to the internal structure of the electric potential (highly radial oscillating solutions remaining absolutely unstable even at very low beam density), has to be added to temperature or dissipative effects which also tend to destroy the absolute character of the instabilities. This effect may become predominant, (even in laboratory experiments,) when the instabilities are sufficiently strong to prevent outer plasma boundaries from playing a significant role in the determination of the mode structure (creation of a radial standing-waves pattern). In determining the outer radial structure of the solutions we have also shown that they look like absolutely unstable modes in the beam's active region only. Outside the beam, the instability is convective, but, due to its backward group velocity (with respect to the beam's direction) it appears to be radially divergent. In the nonpropagative range ($\omega_c < \omega < \omega_p$) the instabilities are weaker but the corresponding electrostatic energy is confined to the beam's region and they will play an important role in the nonlinear development of the electrostatic turbulence and the beam's spreading in energy. In the lower-frequency range ($\omega < \omega_c$) we find convective instabilities with smaller growths, associated with both the Cherenkov and cyclotronic resonance lines.

Our numerical analysis is performed for the parameters of the ARAKS experiment.[1,2] The threshold conditions for obtaining very strong high-frequency turbulence are fullfilled. Many solutions, with the spatio-temporal structure of high-frequency ($\omega \sim \omega_H$), backward-propagating wave packets are then absolutely unstable in the beam's region. They may explain the nontransient part of the high-frequency waves observed during ARAKS flight,[7] which is mainly restricted to the $\omega_p < \omega < \omega_H$ propagative range. On the other hand, the strong high-frequency turbulence ($\omega_c < \omega < \omega_p$) confined to the beam's region may sufficiently spread the beam energy range. Hence, a direct linear mechanism may not explain all the low-frequency whistler waves observed during the ARAKS flight.[7] The observation of these emissions for both backward and upward injections (with respect to the electric receiving antenna) is also an indication of another origin (at least the backward injection). A forthcoming paper will propose a nonlinear antenna's mechanism for the generation of these electrostatic waves [see, in short, Ref. 7(d)].

ACKNOWLEDGMENT

We are gratefully indebted to Dr. D. Pesme for useful discussions and to Dr. A. Roux for pertinent criticisms.

APPENDIX A: THE GREEN'S FUNCTION OF THE WAVE POTENTIAL

Starting from the fluid equations, we set $n = n_{j,0} + n_{j,1} + \cdots$, $\vec{V} = \vec{V}_{j,0} + \vec{V}_{j,1} + \cdots$, and $\Phi = \Phi_0 + \Phi_1 + \cdots$ and obtain

$$\frac{dn_{j,1}}{dt} + \vec{\nabla}\cdot(n_{j,0}\vec{V}_{j,1} + n_{j,1}\vec{V}_{j,0}) = 0\,,$$

$$\frac{d\vec{V}_{j,1}}{dt} + \vec{V}_{j,0}\cdot\nabla\vec{V}_{j,1} + \vec{V}_{j,1}\cdot\nabla\vec{V}_{j,0} = \frac{e}{m}(\vec{\nabla}\Phi_1 - \vec{V}_{j,1}\times\vec{B}_0)\,,$$

$$\Delta\Phi_1 = \frac{e}{\epsilon_0}\sum_j n_{j,1}\,. \tag{A1}$$

j takes different values for the cold-plasma and beam-electron populations. We limit our investigation to a neutralized beam plasma ($\Phi_0 \equiv 0$). The plasma is homogeneous ($n_{p,0} = n_0$) and at rest ($V_{p,0} \equiv 0$). The beam is axial ($\vec{V}_{b,0} = V_b\vec{e}_z$) and has a constant density ($n_{b,0} = n_b$) for $r \leq a$.

We take the Fourier transform of the Euler-Poisson equations with respect to the axial coordinate z and the Laplace transform with respect to time t. After elimination of the density and velocity components we obtain the following equation for the wave potential Φ_1:

$$\frac{1}{r}\frac{d}{dr}\,r\epsilon_\perp(r)\frac{d}{dr}\,\Phi_1 - k_\parallel^2\epsilon_\parallel(r)\Phi_1 = I(r)\,. \tag{A2}$$

As usual in Laplace transforms, I is a cumbersome expression related to the initial conditions $V_{j,1}(r, t=0)$ and $n_{j,1}(r, t=0)$. $\epsilon_\parallel(r)$ and $\epsilon_\perp(r)$ have already been given in Eq. (1a).

To solve the radial nonhomogeneous equation for the wave potential Φ_1 we introduce the Green's function $\tilde{G}(r, r_0, k_\parallel, \omega)$ which is solution of

$$\mathcal{L}\tilde{G} \equiv \frac{1}{r}\frac{d}{dr}\,r\epsilon_\perp(r)\frac{d}{dr}\,\tilde{G} - k_\parallel^2\epsilon_\parallel(r)\tilde{G} = A\delta(r - r_0)\,. \tag{A3}$$

$\tilde{G}$ must be continuous and convergent for all values of r on the inversion path of the Laplace transform: $k_\parallel \in R$ and ω lies above all the singularities of $\tilde{G}$ in the complex ω plane. $\tilde{G}$ is continuous at

the beam boundary

$$\tilde{G}(a_+, r_0, k_\parallel, \omega) = \tilde{G}(a_-, r_0, k_\parallel, \omega)\,, \tag{A4}$$

where $a_\pm = \lim_{\epsilon \to 0}(a \pm \epsilon)$.

The radial derivative of $\tilde{G}$ is discontinuous; the matching conditions are obtained by integration of Eq. (A3) upon r:

$$\epsilon_\perp^{\text{out}} \frac{d}{dr}\tilde{G}(a_+, r_0, k_\parallel, \omega) - \epsilon_\perp^{\text{in}} \frac{d}{dr}\tilde{G}(a_-, r_0, k_\parallel, \omega) = \begin{cases} 0 & \text{if } a \neq r_0 \\ A & \text{if } a = r_0 . \end{cases} \tag{A5}$$

To fulfill the boundary conditions we solve Eq. (A3), respectively, inside the beam ($\tilde{G}$ has to be convergent for $r = 0$) and outside the beam ($\tilde{G}$ has to be convergent for $r \to \infty$). Inside the beam the general solution of Eq. (A3) is given by

$$\tilde{G} = A y_2(r) \int^r dr' \frac{\delta(r' - r_0) y_1(r')}{\epsilon_\perp^{\text{in}} \Delta} + A y_1(r) \int_r dr' \frac{\delta(r' - r_0) y_2(r')}{\epsilon_\perp^{\text{in}} \Delta}\,, \tag{A6}$$

where $y_1(r)$, $y_2(r)$ are two linearly independent solutions of the homogeneous equation $\mathfrak{L}\tilde{G} = 0$ and Δ is the Wronskian of these solutions. Let us now introduce equivalent radial wave numbers inside and outside the beam:

$$k_\perp^{\text{in}} = \left(\frac{\epsilon_\parallel^{\text{in}}}{\epsilon_\perp^{\text{in}}}\right)^{1/2} k_\parallel, \quad k_\perp^{\text{out}} = \left(\frac{\epsilon_\parallel^{\text{out}}}{\epsilon_\perp^{\text{out}}}\right)^{1/2} k_\parallel .$$

For y_1, y_2 we use standard notations for the Bessel functions:

$$y_1(r) = J_0(k_\perp^{\text{in}} r)\,,$$
$$y_2(r) = \lambda J_0(k_\perp^{\text{in}} r) + Y_0(k_\perp^{\text{in}} r)\,, \tag{A7}$$
$$\Delta = 2/\pi(k_\perp^{\text{in}} r)\,.$$

From (A5) and (A6) we obtain

$$\tilde{G} = \begin{cases} \chi^{\text{in}} J_0(k_\perp^{\text{in}} r)[\lambda J_0(k_\perp^{\text{in}} r_0) + Y_0(k_\perp^{\text{in}} r_0)] \text{ for } r < r_0 \\ \chi^{\text{in}} J_0(k_\perp^{\text{in}} r_0)[\lambda J_0(k_\perp^{\text{in}} r) + Y_0(k_\perp^{\text{in}} r)] \text{ for } r > r_0 \end{cases} \tag{A8}$$

with $\chi^{\text{in}} = A\pi(k_\perp^{\text{in}} r_0)/2\epsilon_\perp^{\text{in}}$. Outside the beam

$$\tilde{G} = \chi^{\text{out}} \mu H_0^{(1)}(k_\perp^{\text{out}} r) \tag{A9}$$

with $\chi^{\text{out}} = A\pi(k_\perp^{\text{out}} r_0)/2\epsilon_\perp^{\text{out}}$. Using the connecting conditions (A4) and (A5) to fit the undetermined constant λ and μ one obtains, after straightforward algebra, the expression of the Green's function $\tilde{G}(r, r_0, k_\parallel, \omega)$:

$$\tilde{G} = [1 - Y(r_0 - a)] G_{r_0 < a} + Y(r_0 - a) G_{r_0 > a} + \delta_{(r_0 - a)} G_a\,, \tag{A10}$$

with

$$G_{r_0<a} = \frac{\chi^{\text{in}}}{D}\left([1 - Y(r_0 - r_0)]\psi(r, r_0) + [Y(r - r_0) - Y(r_0 - a)]\psi(r_0, r) + \frac{H_0^{(1)}(k_\perp^{\text{out}} r)}{H_0^{(1)}(k_\perp^{\text{out}} a)} Y(r - a)\psi(r_0, a)\right),$$

$$G_{r_0>a} = \frac{\chi^{\text{out}}}{D}\left(\frac{J_0(k_\perp^{\text{in}} r)}{J_0(k_\perp^{\text{in}} a)}[1 - Y(a - r)]\xi(r_0, a) + [Y(r - a) - Y(r - r_0)]\xi(r_0, r) + Y(r - r_0)\xi(r, r_0)\right),$$

$$G_a = \frac{Aa}{D}\{[1 - Y(r - a)]H_0^{(1)}(k_\perp^{\text{out}} a) J_0(k_\perp^{\text{in}} a) + Y(r - a) H_0^{(1)}(k_\perp^{\text{out}} r) J_0(k_\perp^{\text{in}} a)\},$$

with

$$\psi(r, r_0) = J_1(k_\perp^{\text{in}} r)\{[\Phi_{YJ} + i\Phi_{YY}]J_0(k_\perp^{\text{in}} r_0) - [\Phi_{JJ} + i\Phi_{JY}]Y_0(k_\perp^{\text{in}} r_0)\},$$
$$\xi(r, r_0) = H_0^{(1)}(k_\perp^{\text{out}} r)[\Phi_{JJ} Y_0(k_\perp^{\text{out}} r_0) - \Phi_{YJ} J_0(k_\perp^{\text{out}} r_0)].$$

We have introduced the following quantities:

$$\Phi_{YJ} = \epsilon_\perp^{\text{out}}(k_\perp^{\text{out}} a) Y_0(k_\perp^{\text{in}} a) J_1(k_\perp^{\text{out}} a) - \epsilon_\perp^{\text{in}}(k_\perp^{\text{in}} a) Y_1(k_\perp^{\text{in}} a) J_0(k_\perp^{\text{out}} a)$$

(and straightforward permutation of J and Y for the quantities Φ_{YY}, Φ_{JY}, and Φ_{JJ}). $Y(x)$ is the Heavisides's step function. $D = \Phi_{JJ} + i\Phi_{JY}$ is the dispersion function of the system. The dispersion equation $D = 0$, may consequently be written as in formula (2a) of the text.

An essential point for a correct inversion of the Fourier-Laplace transform is to start with a Green's function converging for $r \to \infty$ along the Bromwich path. This radial convergence implies a "good choice" for the determination of $k_\perp^{\text{out}}$. To make this choice more explicit let us study the function

$$\mathfrak{F}(\omega) = -\frac{\epsilon_\parallel^{\text{out}}}{\epsilon_\perp^{\text{out}}} = -\frac{(\omega^2 - \omega_p^2)(\omega^2 - \omega_c^2)}{\omega^2(\omega^2 - \omega_H^2)} = \left(\frac{k_\perp^{\text{out}}}{k_\parallel}\right)^2 .$$

It is convenient to introduce the variable $x = (\omega^2 - \omega_H^2/2)^2$. Then,

$$\mathcal{F}(\omega) \equiv \mathcal{F}(x) = -\frac{x-(\omega_-)^4}{x-(\omega_+)^4} ,$$

with

$$\omega_- = [(\omega_p^2 - \omega_c^2)/2]^{1/2}, \quad \omega_+ = \omega_H/\sqrt{2} .$$

In the x-plane (see Fig. 12) the loci of constant values of $\arg[\mathcal{F}(x)]$ are pieces of circle passing through the points $A(\omega_-^4, 0)$ and $B(\omega_+^4, 0)$. It is not difficult to map the Laplace-inversion path $\mathcal{L}$ from the ω plane in the x plane (Figs. 13 and 14). The variations of the argument of $\mathcal{F}(x)$ (Fig. 15) when ω follows this Laplace-inversion path show that it is possible to insure convergence for all these paths by choosing the segment AB to be the branch cut of the function $\sqrt{\mathcal{F}(\omega)}$. This is equivalent to assuming the external Green's function ($r > \sup[r_0, a]$) to be proportional to $H_0^{(1)}[ik_\parallel(\epsilon_\parallel^{\text{out}}/\epsilon_\perp^{\text{out}})^{1/2}]$ with the usual branch cutting of the square root on the negative real axis.

APPENDIX B: DEMONSTRATION OF WAVE STABILITY IN THE HIGHER-FREQUENCY WINDOW ($\omega > \omega_H$)

For this demonstration we remove the condition of axis symmetry and the wave potential is taken as $\Phi(r)\exp i(k_\parallel z - \omega t + m\theta)$. We look for unstable Fourier modes (if any) which follow the radial homogeneous differential equation

$$\frac{1}{r}\frac{d}{dr} r\epsilon_\perp(r)\frac{d}{dr}\Phi(r) - \frac{m^2}{r^2}\epsilon_\perp(r)\Phi(r) - k_\parallel^2\epsilon_\parallel(r)\Phi(r) = 0 . \tag{B1}$$

For $\mathrm{Re}[\omega]$ chosen in the nonpropagative frequency range $\mathrm{Re}\,\omega > \omega_H$ and $k_\parallel$ real, we have shown in Appendix A that Φ and $d\Phi/dr$ are vanishing when $r \to \infty$. Multiplying Eq. (B1) by Φ^* and integrating

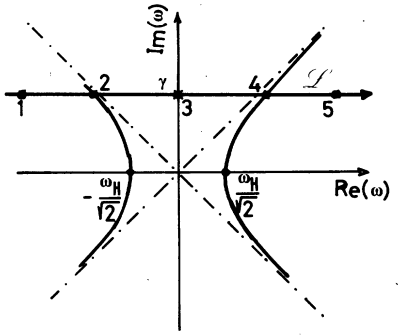

FIG. 13. Inversion path $\mathcal{L}$ for Laplace transform of the Green's function $k_\parallel$ is real and $\mathcal{L}$ is above all the singularities of $\tilde{G}(r, k_\parallel, \omega)$.

by parts upon r we obtain

$$\int_0^\infty \left(\frac{m^2|\Phi|^2}{r^2} + \left|\frac{d\Phi}{dr}\right|^2\right)\epsilon_\perp(r) r\,dr + k_\parallel^2\int_0^\infty \epsilon_\parallel(r)|\Phi^2|r\,dr = 0 ,$$

introducing the positive definite quadratic form (for $k_\parallel$ real):

$$A+ = \int_0^\infty \left(\frac{m^2|\Phi|^2}{r^2} + \left|\frac{d\Phi}{dr}\right|^2\right) r\,dr ,$$

$$A_2 = \int_0^a \left(\frac{m^2|\Phi|^2}{r^2} + \left|\frac{d\Phi}{dr}\right|^2\right) r\,dr ,$$

$$A_3 = \int_0^\infty k_\parallel^2|\Phi|^2 r\,dr ,$$

$$A_4 = \int_0^a k_\parallel^2|\Phi|^2 r\,dr .$$

Equation (B1) may be written in a more convenient form:

$$f(\omega) - \frac{\omega_p^2 A_2}{(\omega - k_\parallel V_b)^2 - \omega_c^2} - \frac{\omega_p^2 A_4}{(\omega - k_\parallel V_b)^2} = 0 , \tag{B2}$$

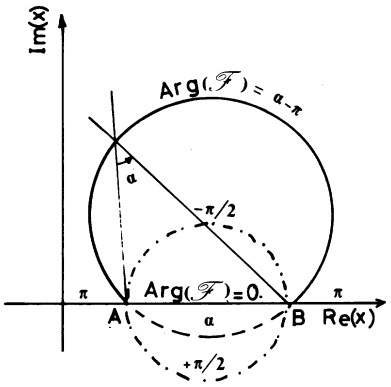

FIG. 12. Loci in x plane where $\arg[\mathcal{F}(x)]$ is constant: $A(\omega_-^4, 0)$; $B(\omega_+^4, 0)$, for $|x| \to \infty$ $\arg\mathcal{F} \to \pi^\pm$.

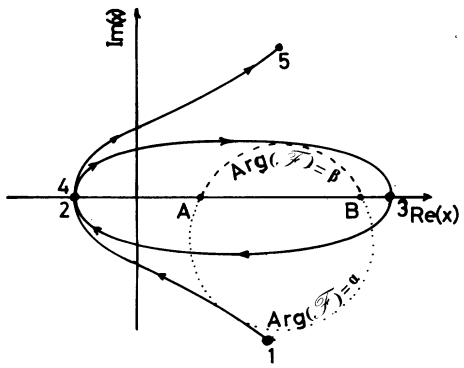

FIG. 14. Mapping of $\mathcal{L}$ into the x plane.

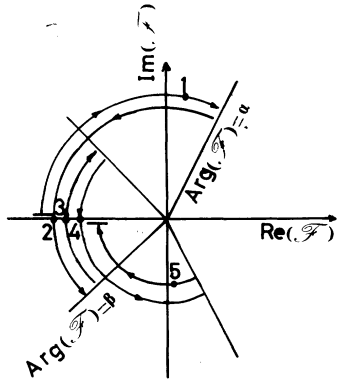

FIG. 15. Variations of $\arg[\mathfrak{F}(\omega)]$ for ω on $\mathfrak{L}$.

with

$$f(\omega)=A_1(\omega^2-\omega_H^2)/(\omega^2-\omega_c^2)+A_3(\omega^2-\omega_p^2)/\omega^2 .$$

We look for unstable Cherenkov modes and set $\omega=\omega_0+\delta\omega$ with $\omega_0=k_\parallel V_b$ (the demonstration is similar for the cyclotronic modes). We expand Eq. (B2) in powers of $\delta\omega$ and obtain

$$f(\omega_0)S\omega^4-[\omega_c^2 f(\omega_0)+\omega_p^2(A_2+A_4)]+A_4\omega_p^2\omega_c^2=0 . \quad \text{(B3)}$$

For $\omega_0>\omega_H$ $f(\omega_0)$ is positive; the discriminant, the product, and the sum of the two roots of the biquadratic equation (B3) are all positive and definite. The four roots of Eq. (B3) are real and the waves are stable.

APPENDIX C: ANALYTICAL CRITERION FOR ABSOLUTE INSTABILITY IN THE HIGH-FREQUENCY WINDOW ($\omega_p<\omega<\omega_H$)

In a similar previous work[11] the analytical criterion for an absolute Cherenkov instability was obtained by expansion in powers of ϵ (ϵ is the ratio between the beam and plasma densities). This expansion is *a priori* possible when the beam-plasma system is confined by a waveguide with a finite radius $r=b$: in this case a set of radial plasma modes exists without beam. Nevertheless, we have already pointed out in part I of this work that this expansion is only justified when the beam plasma is not confined by a waveguide, the radial normal modes are determined by the beam and one has to find a different procedure.

To simplify the algebra we limit our investigation to solutions which have a large number of radial nodes inside the beam. This simplification allows a plane-sheet beam model. In our analytical treatment we apply directly the Bers-Briggs criterion for absolute instability[19]: We establish the analytical condition for the occurrence of a saddle point in the complex $k_\parallel$ plane (with $\mathrm{Im}\omega>0$ and $\mathrm{Im}k_\parallel<0$). We also verify that such a saddle point is produced by the merging of two branches of the dispersion relation which for $\mathrm{Im}k_\parallel=0$ corresponds both to $\mathrm{Im}\omega>0$.

Solving the Euler-Poisson equations in plane geometry, as already done in Appendix A for the cylindrical case, we easily obtain the following set of equations:

$$S^2z^2\epsilon_\parallel^{in}+T^2\epsilon_\perp^{in}=0 , \quad \text{(C1a)}$$

$$S^2z^2\epsilon_\parallel^{out}+U^2\epsilon_\perp^{out}=0 , \quad \text{(C1b)}$$

$$T\,\mathrm{tg}T=-iU\frac{\epsilon_\perp^{out}}{\epsilon_\perp^{in}} , \quad \text{(C1c)}$$

with

$$\epsilon^{in}(\epsilon)=1-\frac{1}{\alpha^2}-\frac{\epsilon}{(z-\alpha)^2}\,\epsilon^{out}=\epsilon^{in}(0) ,$$

$$\epsilon_\perp^{in}(\epsilon)=1-\frac{1}{\alpha^2-\alpha_c^2}-\frac{\epsilon}{(z-\alpha)^2-\alpha_c^2}\,\epsilon_\perp^{out}=\epsilon_\perp^{in}(0) ,$$

$$z=k_\parallel V_b/\omega_p , \quad S=\omega_p a/V_b , \quad \alpha=\omega/\omega_p .$$

The dispersion relation would follow by elimination of U and T as given by (C1a) and (C1b) into (C1c). Equation (C1c) shows that a set of branches of Cherenkov modes may be associated one by one to the sheets of the Riemann surface of the multivalued function $\tan T$. To each sheet corresponds an interval of π for the real T values [ReT between $k\pi$ and $(k+1)\pi$, k being the number of nodes of the corresponding solution inside the beam radius].

To find a saddle point eventually associated to an absolute instability, we look for a solution of the dispersion relation such that $\partial\alpha/\partial z=0$. It is convenient to take the derivative of (C1) with respect to z. $\partial T/\partial z$ gives a negligible correction for U and T large. As a result we obtain

$$z\frac{S^2}{T^2}\left(1-\frac{1}{\alpha^2}+\frac{\alpha\epsilon}{(z-\alpha)^2}\right)+\frac{\epsilon(z-\alpha)}{[(z-\alpha)^2-\alpha_c^2]^2}=0 . \quad \text{(C2)}$$

In the following, we assume a tenuous beam, with $\epsilon\ll\alpha_c^2$ and $\alpha_c^2\ll 1$, which corresponds to ionospheric conditions.

To solve Eqs. (C1) and (C2) we assume at first $|T|/S\gg 1$ ($k_\perp^{in}\gg\omega_p/V_b$), which implies solutions with a large number of internal nodes. Then according to values of the small parameter $\epsilon/\alpha_c^2(\eta)$, (C2) may be easily solved. For $\eta T^2/S^2<1$ we obtain

$$z-\alpha=\eta^{1/3}\left(1+\frac{T^2}{S^2}\,\xi\right)^{1/3}e^{(2n+1)i\pi/3}, \quad (n=0,1,2) \quad \text{(C3a)}$$

where $\xi\sim 0$ if $\eta^{1/3}<\alpha_c$ and $\xi\sim 1$ if $1>|T^2/S^2\eta|^{1/3}>\alpha_c$. In the opposite case, for $\eta T^2/S^2>1$,

$$z-\alpha=(\eta T^2/S^2)^{1/4}e^{(2m+1)i\pi/4}-\tfrac{1}{4} \quad (m=0,1,2,3) . \quad \text{(C3b)}$$

We proceed with the solution of (C1a) and get

$$\alpha = \alpha_H - \frac{1}{2}\frac{S^2}{T^2}\alpha_c^2 \times \left[1 + 3\eta^{1/3}\left[\frac{1 + \left(\frac{2\xi + \sqrt{\xi}}{3}\right)\frac{T^2}{S^2}}{\left(1 + \xi\frac{T^2}{S^2}\right)^{2/3}}\right] e^{(2n+1)i\pi/3}\right], \quad \text{(C4a)}$$

for cases covered by formula (C3), and

$$\alpha = \alpha_H - (-1)^m \frac{S}{T} i\eta^{1/2}\left[1 + \frac{1}{\eta^{1/4}}\left(\frac{S}{T}\right)^{1/2} e^{-(2m+1)i\pi/4}\right], \quad \text{(C4b)}$$

when (C3b) applies. In all these cases, the frequency at which a double root occurs lies close to the upper hybrid frequency. The necessary conditions for an absolute instability ($\mathrm{Im} z < 0$) imply $n = 2$ and $m = 3$ (T being essentially real). From (C1b) we then compute a relation between the inner and outer radial wave numbers

$$U = T\left(1 - \frac{\eta^{1/3}}{2}\frac{1 + \sqrt{\epsilon}\,T^2/S^2}{(1 + \xi T^2/S^2)^{2/3}} e^{-i\pi/3}\right), \quad \text{(C5a)}$$

$$U = \frac{T}{\sqrt{2}}\left[1 + \frac{1}{4}\frac{1}{\eta^{1/4}}\left(\frac{S}{T}\right)^{1/2} e^{i\pi/4}\right]. \quad \text{(C5b)}$$

In (C5a) [(C5b)] we have assumed $\mathrm{Re}(U)$ and $\mathrm{Re}(T)$ positive, which is necessary for an outgoing wave. To achieve the solution of Eqs. (C1), we eliminate U between (C5a) (C5b), and (C1c) and compute T:

$$T = (l + \tfrac{1}{6})\pi + \frac{i}{2}\ln\{\tfrac{1}{4}\eta^{1/3}\}, \quad (\text{if } \eta^{1/3} < \alpha_c), \quad \text{(C6a)}$$

$$T = (l - \tfrac{1}{3})\pi + \frac{i}{2}\ln[\tfrac{1}{4}\eta^{1/3}(1 + T^2/S^2)^{1/3}] \quad [\text{if } 1 > (\eta T^2/S^2)^{1/3} > \alpha_c], \quad \text{(C6b)}$$

$$T = \pi(l - \tfrac{1}{2})\pi + \frac{i}{2}\ln\left(\frac{\sqrt{2} - 1}{\sqrt{2} + 1}\right)\left(\text{if } \eta\frac{T^2}{S^2} > 1\right). \quad \text{(C6c)}$$

At this stage, by substitution of the values of T into (C4a) [(C4b)] we obtain the necessary condition for instability ($\mathrm{Im}\,\alpha > 0$), which reads simply

$$\frac{\eta}{S^2} > \zeta(A)A^3, \quad \text{(C7)}$$

where $A = \ln 6\sqrt{3}\,T_r/6\sqrt{3}\,T_r$ and $\zeta = (8/T_r)^2$, if $A > \alpha_c/4$, and $\zeta = (8/S)^2$, if $A \ll \alpha_c/4$, and T_r is the real part of T. Moreover, by substitution of T in (C5a) [(C5b)] we may deduce the sign of the imaginary part of U. We see that $\mathrm{Im}(U)$ is positive for

$$\xi(B)B^3 < \frac{\eta}{S^2} \leq (T_r/25)^2, \quad \text{(C8)}$$

where $B = \ln 2\sqrt{3}\,T_r/2\sqrt{3}\,T$. In this parameter range the solution corresponds to a radially convergent normal mode which is absolutely unstable (if all the Bers-Briggs conditions are fulfilled). As condition (C7) is less restrictive than (C8) we may also obtain a solution which is divergent ($\mathrm{Im} U < 0$) outside the beam, and corresponds to a radially amplified wave packet. The instability is then absolute inside the beam, but not outside. In this second region the apparent radial amplification is due to the negative axial group velocity in the background plasma, as explained in the first part of the paper.

To fulfill the last Bers-Briggs condition we look at the solution of the dispersion equation (C1) for $\mathrm{Im}\,\alpha$ growing to $+\infty$ and obtain three branches, two Cherenkov branches

$$z \simeq \alpha\left(1 \pm \frac{S\sqrt{\epsilon}}{\sqrt{S^2\alpha^2 - T^2}}\right), \quad T \simeq (l + \tfrac{1}{2})\pi + \frac{i}{2}\ln(\tfrac{1}{4}), \quad \text{(C9)}$$

and a plasma branch determined by the connecting conditions at the beam surface:

$$T \simeq U \simeq iSz$$

and

$$Sz \simeq -i(l + \tfrac{1}{2})\frac{\pi}{S} + \frac{1}{2S}\ln\left(\frac{\epsilon}{2|\mathrm{Im}\,\alpha|^2}\right). \quad \text{(C10)}$$

This branch together with one of the beam's branches forms a saddle point, hence, giving rise to an absolute instability. This nonconvective instability disappears for $\epsilon < \epsilon^I$, the threshold value for the beams density which can be computed from (C7).

---

*Equipe de Recherche du CNRS No. 174.

[1]J. R. Winckler Cosm. Phys. Technical Report No. 168, University of Minnesota, Minneapolis, 1976 (unpublished).

[2]F. Cambou, J. Lavergnat, V. V. Migulin, A. I. Mozorov, B. E. Paton, R. Pellat, A. K. Pyatsi, M. Reme, R. Z. Sagdeev, W. R. Sheldon, and I. A. Zhulin, Nature (London) 271, p 723 (1978).

[3]J. V. Alekhin, V. I. Karpman, D. J. Rjutov, and R. Z. Sagdeev, Cos. Elec. 2, 280 (1971).

[4]D. G. Cartwright and P. J. Kellogg, J. Geophys. Res. 79, 1439 (1974).

[5]J. Lavergnat and R. Pellat, J. Geophys. Res. 84, 7223 (1979).

[6]J. Lavergnat, Ph.D. thesis, University of Paris XI, 1976 (unpublished).

[7]Ann. Geophys. 36, (1980). All this issue is a review of the experimental results of the ARAKS experiment. See, in particular, (a) J. Lavergnat, M. Dechambre, R. Pellat, Yu. V. Kushnerevsky, and S. A. Pulinets

(p. 323); (b) M. Dechambre, G. A. Gusev, Yu. V. Kushnerevsky, J. Lavergnat, R. Pellat, S. A. Pulinets, V. V. Selegei, and I. A. Zhulin (p. 333); (c) M. Dechambre, Yu. V. Kushnerevsky, J. Lavergnat, R. Pellat, S. A. Pulinets, and V. V. Selegei (p. 341); (d) J. Lavergnat, D. Le Queau, A. Roux, and R. Pellat (p. 439).

[8]P. A. Sturrock, Phys. Rev. 117, 1426 (1960).

[9]R. Pellat, J. Lavergnat, and A. Saint Marc, C. R. Acad. Sci. (Paris) 282(B), 201 (1976).

[10]J. Lavergnat, D. LeQueau, R. Pellat, and A. Roux, C. R. Acad. Sci. (Paris) 284(B), 417 (1977).

[11]J. Manickam, W. Carr, B. Rosen, and M. Seidl, Phys. Fluids 18, 369 (1975).

[12]A. B. Kitsenko and M. M. Shoucri, Plasma Phys. 10, 23 (1968).

[13]M. M. Shoucri and A. B. Kitsenko, Plasma Phys. 10, 699 (1968).

[14]J. E. Simpson and D. A. Dunn, J. Appl. Phys. 37, 4201 4201 (1966).

[15]G. Bekefi, *Radiation Processes in Plasma* (Wiley, New York, 1970).

[16]J. Y. Delahaye, J. Lavergnat, R. Ney, and J. F. Karczewski, Space Sci. Instrum. 4, 413 (1978).

[17]S. Bliman and A. Bouchoule, J. Appl. Phys. 38 5065 (1967).

[18]A. Bers, *Proceedings of the Summer School at Les Houches*, edited by C. DeWitt and J. Peyraud (Gordon and Breach, New York, 1972).

[19]A. I. Akhiezer and R. V. Polovin, Usp. Fiz. Nauk 104, 185 (1977) [Sov. Phys.—Usp. 14, 278 (1971)].

[20]K. B. Dysthe, Nucl. Fusion 6, 215 (1966).

[21]M. F. Gorbatenko, Zh. Tekh. Fiz. 33, 1070 (1963) [Sov. Phys.-Tech. Phys. 8, 798 (1964)].

[22]P. M. Morse and H. Feshback, *Methods of Theoretical Physics* (McGraw-Hill, New York, 1965).

[23]D. E. Muller, Math. Tab. Aids Comput. 10, 208 (1956).

[24]L. S. Hall and W. Heckrotte, Phys. Rev. 166, 120 (1968).